Loss of tumor suppressor *NF1* activates HSF1 to promote carcinogenesis

Chengkai Dai[1,3,6,7], Sandro Santagata[1,2,7], Zijian Tang[3] Jiayuan Shi[3], Junxia Cao[3], Hyoungtae Kwon[1], Roderick T. Bronson[4], Luke Whitesell[1], and Susan Lindquist[1,5,6]

[1]Whitehead Institute for Biomedical Research, Cambridge, MA 02142, USA;

[2]Department of Pathology, Brigham and Women's Hospital, Boston, MA 02115, USA;

[3]The Jackson Laboratory, Bar Harbor, ME 04609, USA;

[4]Department of Pathology, Tufts University School of Medicine and Veterinary Medicine, Boston, MA 02155, USA;

[5]Howard Hughes Medical Institute and Department of Biology, Massachusetts Institute of Technology, Cambridge, MA 02139, USA

[6]Corresponding authors
Chengkai Dai, The Jackson Laboratory, Bar Harbor, ME 04609, USA
E-mail: Chengkai.Dai@jax.org; Phone (207)288-6927; FAX (207) 288-6078
Susan Lindquist, Whitehead Institute for Biomedical Research, Cambridge, MA 02142, USA
E-mail: Lindquist_admin@wi.mit.edu ; Phone (617) 258-5184; FAX (617) 258-5737

[7] These authors contributed equally to this work.

Running Title: *NF1* loss activates HSF1

Keywords: Neurofibromatosis, NF1, Heat-shock, HSF1, Carcinogenesis, MPNST

The authors have declared that no conflict of interest exists.

Abstract

Intrinsic stress response pathways are frequently mobilized within tumor cells. The mediators of these adaptive mechanisms and how they contribute to carcinogenesis remain poorly understood. A striking example is Heat Shock Factor 1 (HSF1), master transcriptional regulator of the heat-shock response. Surprisingly, we find that simple compromise of a tumor suppressor, *Neurofibromatosis Type 1* (*NF1),* increases HSF1 levels and triggers its activation. As a consequence, *Nf1*-null cells acquire tolerance to proteotoxic stress. This activation of HSF1 depends on dysregulated MAPK signaling. HSF1 in turn supports MAPK signaling. In mice, *Hsf1*-deficiency impedes NF1-associated carcinogenesis by attenuating oncogenic RAS/MAPK signaling. In cell lines from human Malignant Peripheral Nerve Sheath Tumors (MPNSTs) driven by *NF1* loss, HSF1 is over-expressed and activated. This activation is required for tumor cell viability. In surgical resections of human MPNSTs, HSF1 is over-expressed, translocated to the nucleus and phosphorylated. These findings reveal a surprising new biological consequence of *NF1*-deficiency: activation of HSF1 and an ensuing addiction to this master regulator of the heat-shock response. The loss of this tumor suppressor's function engages an evolutionarily conserved cellular survival mechanism that, ironically, impairs survival of the whole organism by facilitating carcinogenesis.

Introduction

Evolutionarily conserved from yeasts to humans, the heat-shock transcription factor, HSF1, is activated by a broad range of stressors that extend far beyond heat, including heavy metals, UV radiation, hypoxia, desiccation, and acidosis (1). During activation, HSF1 undergoes phosphorylation and other post-translational modifications, trimerization and nuclear translocation. This results in rapid, high affinity binding of HSF1 to consensus Heat Shock Elements (HSE) within the promoters of target genes (2). Such binding drives the induction or suppression of hundreds of genes in mammalian cells (3).

The adaptive response that is unleashed by HSF1 activation is critical for maintaining homeostasis of the cell's proteome, mediated in large part by increased expression of classical heat-shock proteins such as HSP27, HSP70 and HSP90 (4). However, the impact of HSF1 activation goes far beyond these chaperones. It helps coordinate a range of fundamental cellular processes that are important to the fitness of malignant cells including cell cycle control, ribosome biogenesis, protein translation, and glucose metabolism (5). As a result, HSF1 both facilitates initial oncogenic transformation and also maintains the malignant phenotype of established cancer cell lines driven by a wide range of mutations. In mice and cell culture, genetic ablation of *Hsf1* expression potently impairs tumorigenesis and cellular transformation driven by oncogene activation or tumor suppressor loss (5). The importance of HSF1 in enabling malignancy has been demonstrated by other recent work as well (6-8). Given the importance of HSF1 in diverse survival mechanisms and cancer, we sought here to investigate factors that might increase its transcriptional activity during tumorigenesis.

Neurofibromatosis Type 1 (NF1) is a common hereditary cancer syndrome associated with dysregulation of RAS activity (9). Tumor predisposition results from loss-of-function mutations in the *NF1* gene, which encodes neurofibromin, a 280 kD protein possessing a central domain with Ras GTPase Activating Protein (GAP) activity (10). Consistent with neurofibromin functioning as a negative regulator of RAS, *NF1*-deficient cells are hyper-responsive to several growth factors that signal via the

RAS/MAPK pathway (11). Indeed, when over-expressed, the GAP-related domain (NF1-GRD) can down-regulate RAS-mediated mitogenic signaling (12).

Unexpectedly, we found that the tumor suppressor *Nf1* is a strong regulator of HSF1 levels and activity. Indeed, genetic compromise of *Nf1* is alone sufficient to cause an immediate activation of HSF1 in cell culture. HSF1 levels are also increased in tumor samples removed directly from NF1 patients. Having found that *Nf1* regulates HSF1 function, we investigated the underlying mechanism(s) of this control as well as its functional consequences. We demonstrate that HSF1 is embedded in the dysregulated MAPK/RAS signaling that is characteristic of NF1, and that HSF1 participates in a feed-forward loop that facilitates tumorigenesis in mice and humans. Based on these findings, HSF1 now emerges as a previously unsuspected but clinically relevant modifier of NF1-associated tumorigenesis.

Results

Nf1-deficiency up-regulates HSF1 and activates the heat-shock response

Given the importance of HSF1 in supporting tumorigenesis we sought to identify genes that might modulate HSF1 function and the transcriptional response that it regulates. We screened a focused library of lentiviral inhibitory short hairpin RNAs (shRNAs) targeting 175 genes that were selected based on 1) Gene Ontology or Panther annotation under the categories of heat-shock, stress response, sensitivity to stress, protein folding or protein degradation and 2) iHOP interactome data indicating direct interaction with HSF1 (Supplemental Figure 1). NF1 was added to the list because a deletion mutation of its yeast homolog reduces thermotolerance in that organism (13).

HSF1 activation was monitored using NIH3T3 cells stably engineered to express an eGFP-firefly luciferase fusion controlled by a highly HSF1-dependent promoter (14). Luminescence per well was recorded five days post lentiviral transduction. As expected, shRNAs targeting *Hsp27/Hspb2*, *Hsp47/Serpinh1*, α(B)-crystallin*/Cryab* and several *Hsp40* family members (*Dnajb6* and *Dnajc17*) strongly activated the heat-shock reporter (Figure 1A). Hairpins targeting individual *Hsp90* and *Hsp70* isoforms resulted in only weak reporter induction, most likely because shRNA targeting of individual isoforms may be insufficient to impair function of the many isoforms comprising the HSP70 and HSP90 class of chaperones. Surprisingly, two independent *Nf1*-targeted shRNA hairpins were among the very strongest activators.

Next, we examined the impact of stable *Nf1* knockdown on the activation of HSF1 in a mouse embryonic fibroblast (MEF) cell line immortalized with the HPV16 E6/E7 oncoproteins (6). Compared to a scrambled (Scram) control shRNA, two independent shRNAs (#39 and #42) efficiently suppressed the neurofibromin protein levels and induced an increase in the level of the heat-shock protein HSP72, a classic HSF1 target (Figure 1B). The hairpin that suppressed neurofibromin expression most efficiently (#42) also induced the strongest expresson of HSP72. We further examined transcript levels

of HSF1 target genes by real-time quantitative RT-PCR analysis in these *Nf1*-knockdown cells. Compared to the control, knockdown of *Nf1* by both #39 and #42 shRNAs increased transcript levels of a collection of *Hsp* genes including *Hsp70s* (*Hsp72*/*Hspa1a* and *Hspa4l*), *Hsp40s* (*Dnajb1* and *Dnajb2*), *Hsp90* (*Hsp90aa1*) and a small *Hsp* family member (*Hspb8*) (Figure 1C). Hairpin #42 induced the strongest expression of these *Hsp* genes. These results demonstrate that reducing *Nf1* expression can activate the heat-shock response in pre-malignant cells.

To measure the effect of *Nf1*-targeted hairpins on HSF1 protein levels, we immunoblotted lysates (Figure 2, A and B) from the same stably transduced *Nf1*-knockdown cells. HSF1 normally shuttles between the nucleus and cytoplasm, but differential residence time in these compartments results in predominantly cytoplasmic localization under basal conditions. Upon activation, however, HSF1 accumulates in the nucleus where a portion becomes tightly bound to DNA (Supplemental Figure 2A). Both #39 and #42 shRNAs increased HSF1 levels and translocation of HSF1 to the nucleus compared to the control shRNA (Figure 2, A and B). They also induced phosphorylation of HSF1 at serine residue 326 (p-S326) (Figure 2, A and B), a modification that is strongly associated with HSF1 activation in vivo by thermal and chemical stressors (15). The kinases or signaling pathways responsible for this key modification has yet to be defined, but consistent with activation of HSF1 by stable *Nf1* knockdown, HSP72 protein levels were elevated (Figure 2B). The transcript level for *Hsf1* was not altered by *Nf1*-knockdown (Supplemental Figure 2B), suggesting post-transcriptional regulation of HSF1 levels.

To confirm the effects demonstrated by shRNA knockdown experiments, we further tested the effect of *Nf1*-deficiency using primary MEFs in which the *Nf1* locus was disrupted by gene-targeting. Primary cultures derived from both *Nf1* heterozygous (*+/-)* and null (*-/-)* embryos had increased HSF1 protein levels compared to their wild-type (*+/+)* counterparts (Figure 2, C and D). Null cells displayed even higher levels of HSF1 protein and greater induction of HSP72 than heterozygous cells (Figure 2,

C and D). *Nf1*-null cells also had an increase in both nuclear HSF1 and the activating p-S326 modification than wild-type cells (Figure 2D).

Dysregulated MAPK signaling mediates HSF1 activation

How might *Nf1* loss increase p-S326, nuclear accumulation of HSF1 and total HSF1 levels? A hallmark of the NF1 phenotype is dysregulation of RAS activation with downstream effects on the MAP kinase/ERK (MAPK/ERK) signaling cascade. Hence, *Nf1* loss could activate HSF1 through the MAPK pathway. We tested this possibility using U0126, a potent and selective inhibitor of MAP Kinase Kinase (MEK1 and 2), the immediate upstream activators of ERK 1 and 2. U0126 reduced activation-associated phosphorylation of HSF1 as well as its nuclear accumulation, leading to a decline in HSP72 levels in both control and *Nf1*-knockdown cells (Figure 2B). Interestingly, U0126 had a greater effect on *Nf1*-knockdown cells than on control cells (Supplemental Figure 2C). U0126 exhibited similar effects on primary *Nf1-/-* MEFs to those seen in knockdown cells (Figure 2D and Supplemental Figure 2D). The compound also caused an increase in HSF1 phosphorylation and HSP72 level in primary *Nf1*+/+ MEFs (Figure 2D). This likely reflects a biological difference between immortalized and primary cells. Either blocking this trophic signaling pathway is stressful to primary, *Nf1*-wild type cells or basal MAPK activities actually repress HSF1 activation in these cells. In any case, the data in *Nf1*-deficient cells indicate that hyperactivated MAPK signaling contributes to HSF1 Ser326 phosphorylation, nuclear translocation and activation.

Next we used a heat-shock reporter assay to examine the effect of dysregulated MAPK signaling on HSF1 transcriptional activity in HEK293T cells. In the absence of environmental insults, the transfected reporter demonstrated a modest level of activation that was further enhanced by overexpression of HSF1 (Figure 2E). Inhibition of endogenous MEK activity by U0126 significantly suppressed both basal and HSF1-driven reporter activity (Figure 2E). To further validate the role of hyperactive MAPK signaling in HSF1 phosphorylation and activation, we transiently transfected HEK293T cells with a

dominant negative MEK1 mutant ($MEK1^{AA}$), in which two key serine residues at 218 and 222 are substituted with alanine (16). In agreement with our U0126 data, expression of $MEK1^{AA}$ impaired HSF1 Ser326 phosphorylation as well as HSF1-mediated reporter activation (Figure 2, F and G). Although significant, mutant MEK1 reduced reporter activity less than U0126. This is likely due to both the limited efficiency of HSF1 and $MEK1^{AA}$ co-transfection and the potential for MEK2 compensatory effects. Together these data indicate that MEK hyperactivation is important for HSF1 S326 phosphorylation and activation.

Does MAPK signaling also underlie the increase in total HSF1 protein? Because HSF1 mRNA is not increased in NF1-deficient cells, we investigated post-transcriptional mechanisms that might contribute to increasing HSF1 protein after *NF1* loss. Interestingly, HSF1 levels in control cells (Scr) increased by more than two-fold following proteasome inhibition with MG132 but there was only subtle change in HSF1 levels in *Nf1*-knockdown cells (#42) (Figure 2H and Supplemental Figure 2E). This finding suggested that HSF1 is a substrate for the proteasome but that its degradation is impaired in *Nf1*-deficient cells.

To further explore the impaired degradation of HSF1 in *Nf1*-deficient cells and to establish a link to MAPK signaling, we immunoprecipitated polyubiquitinated HSF1 from control and *Nf1*-knockdown cells (17). While polyubiquitinated HSF1 was readily detected in control cells (Scr), HSF1 polyubiquitination was markedly diminished in *Nf1*-knockdown cells (#42) (Figure 2I). Strikingly, inhibiting MEK with U0126 re-established polyubiquitination of HSF1 (Figure 2I). Thus, MEK hyperactivation also regulates HSF1 polyubiquitination and proteasomal degradation.

HSF1 activation by *Nf1* loss induces stress tolerance

Next we asked if loss of *Nf1* alone, and subsequent activation of HSF1, might be sufficient to provide cells with a survival advantage in the face of increased levels of proteotoxic stress. To test this, we

generated primary MEFs from mice carrying targeted *Hsf1* or *Nf1* knockouts. Because the *Nf1*-/- genotype is embryonic lethal (18) and *Hsf1*-/- mice have reproductive defects (19), it was necessary to screen over 120 embryos in order to isolate MEFs with four distinct genotypes: *Hsf1*+/+ cells that were either *Nf1*+/+ or *Nf1*-/- and *Hsf1*-/- cells that were *Nf1*+/+ or *Nf1*-/-. We then measured the changes in cell number in the presence of three chemically and mechanistically distinct cellular stressors: the proteasome inhibitor MG132 (Figure 3A), the HSP90 inhibitor radicicol (Figure 3B) and the thiol-reactive compound Withaferin A (WA) (Figure 3C) (20, 21). Unlike the situation in yeast where deletion of the *Nf1* homolog *IRA2* reduces thermotolerance, MEFs lacking *Nf1* (*Hsf1*+/+,*Nf1*-/- MEF) were significantly more resistant to all three proteotoxic stressors than wild-type MEFs (Figure 3, A-C). In fact, *Hsf1*+/+,*Nf1*-/- MEFs showed an increase in cell number at low concentrations of MG132 and WA. In contrast, disrupting *Nf1* in *Hsf1*-/- cells did not confer resistance to the stressors (Figure 3, A-C). Thus, the tolerance of *Nf1*-deficient cells to proteotoxic stress is mediated by *Hsf1*.

***Hsf1* compromise suppresses tumorigenesis in mice**

Because tumorigenesis imposes diverse stresses on the physiology of cells, we wondered whether HSF1 activation and the ensuing acquisition of tolerance to proteotoxic stress could facilitate NF1-associated tumorigenesis in vivo. To investigate, we turned to *NPcis* mice. The tumor predisposition syndrome caused by *NF1* loss in humans has proven difficult to faithfully model in mice. Homozygous germline disruption of the *Nf1* gene is embryonic lethal predominantly due to defects in cardiovascular system development (22). Heterozygous mice display modest tumor predisposition, but they do not develop the classic spectrum of lesions characteristic of the human disease, especially neurofibroma and MPNST (23). The observation that the tumor suppressor *TP53* is frequently lost in human MPNSTs prompted development of mouse models in which alleles of the closely linked *Trp53* and *Nf1* genes are disrupted on the same chromosome (24, 25). The chromosome bearing deletion of both *Nf1* and *Trp53* in *cis* is designated *NPcis*. Heterozygotes (*NPcis*+/-) develop soft tissue sarcomas resembling human MPNSTs with high frequency. Due to the close proximity of the *Trp53* and *Nf1* genes (in humans as

well as mice), such tumors often demonstrate loss of heterozygosity (LOH) for the remaining wild-type alleles of both genes.

To examine the effect of HSF1 in this model, we crossed *NPcis+/-* mice with *Hsf1+/-* mice. *NPcis+/-, Hsf1+/-* offsprings were intercrossed to produce the following genotypes: 1) *NPcis+/+, Hsf1+/+;* 2) *NPcis+/+, Hsf1-/-;* 3) *NPcis+/-, Hsf1+/-;* 4) *NPcis+/-, Hsf1-/-;* and 5) *NPcis+/-, Hsf1+/+*. Genotypes 1 and 2 served as controls for the effect of *Hsf1* knockout on otherwise wild-type mice. As expected these control mice had long-term tumor-free survival (Figure 4A). Genotypes 3, 4 and 5 tested for the effect of *Hsf1* dosage on tumorigenesis in the *NPcis* background. All *NPcis* mice with wild-type *Hsf1* developed tumors by about 250 days, with a median tumor-free survival of only 154 days (Figure 4A). In contrast, *NPcis* mice with hemizygous or homozygous *Hsf1* knockout both enjoyed significantly prolonged tumor-free survival, with median survivals of 235 and 206 days respectively.

The difference in tumor-free survival between homozygous and heterozygous *Hsf1* knockouts, however, was not statistically significant. This contrasts with our previous results in mice carrying a hotspot mutation in *Trp53.* In that case *Hsf1*-heterozygous mice also had improved outcome compared to *Hsf1*-wild type mice, but *Hsf1*-null mice survived even longer. While being a prominent longevity factor in nematodes (26, 27), the influence of HSF1 on mammalian lifespan has been little explored. In some strains, *Hsf1* compromise has no effect on lifespan (5, 28). However, we find that in the mixed background used for our *NPcis* experiments, *Hsf1* knockouts had a shorter lifespan than wild type controls. This effect is evident in the depiction of overall survival provided in supplemental Figure 3A which includes deaths from all causes, not solely tumor-related deaths as used for analysis of tumor-free survival (Figure 4A). Thus, the additional survival advantage that might have been conferred on tumor-associated mortality by loss of the second *Hsf1* allele was likely masked by general effects of *Hsf1* on lifespan in the *NPcis* strain.

To characterize the tumors arising in *NPcis* mice we first examined their HSF1 status. In the same sections, MPNST tumor cells had much stronger HSF1 immunoreactivity than adjacent normal tissues such as nerve (NV; Figure 4B). The absence of reactivity in tumors arising in *Hsf1*-null mice confirmed the specificity of the HSF1 staining.

NF1 patients can develop a broad range of tumor types, most of which also occur in *NPcis* mice (Supplemental Figure 4). To capture all tumor types arising in this model a full necropsy was performed on each euthanized animal and all major tissues were harvested for histological examination. In addition to prolonging tumor-free survival, *Hsf1*-deficiency altered the distribution of tumor types arising in this model. Compared to *Hsf1* wild-type mice, the incidence of lymphoma, neuroblastoma, angiosarcoma, osteosarcoma, pheochromocytoma, and histocytic sarcoma were all reduced in *Hsf1* null mice (Supplemental Figure 3B). Surprisingly, the overall incidence of MPNSTs and gliomas was not significantly different. Excluding gliomas and MPNSTs, however, tumor incidence was significantly lower in *Hsf1* null mice (5.9%) and *Hsf1* hemizygous mice (26.9%) mice compared to *Hsf1* wild-type mice (60.9%). The MPNST arising in *Hsf1* +/+, +/- and -/- tumors appeared histologically similar.

Although MPNST incidence did not differ, *Hsf1*-deficiency did prolong survival time in mice that only developed MPNSTs (Figure 4C). This effect was statistically significant in *Hsf1* hemizygous mice ($p=0.0152$), and there was a trend toward significance in *Hsf1*-null mice ($p=0.0869$). Given the late-occurring, slowly progressing behavior of glioma in this *NPcis* model, the apparent increase in glioma incidence in *Hsf1*-deficient mice is likely due simply to their prolonged survival. Indeed, there was a strong positive correlation between glioma incidence and median survival across *Hsf1* genotypes (Supplemental Figure 3C).

To circumvent placental defects associated with the *Hsf1* null state in highly inbred genetic backgrounds (19), *Hsf1* mice were maintained on a mixed genetic background (129/SvJ and Balb/cJ).

Previously two genetic loci, mapping to chromosome 15 and 19 respectively, as well as sex-specific effects have been reported to modify tumorigenesis in the *NPcis* model (29,30). To address potential confounding effects of these modifiers in our study, we examined the correlation of mapped genetic loci or sex with animal survival (Supplemental Table, 1 and 2). Neither the states of these loci nor sex demonstrated a significant effect on survival (Supplemental Figure 5). Taken together, our data establish *Hsf1* as a previously unreported modifier of NF1-associated tumorigenesis in this mouse model.

HSF1 supports MAPK/ERK signaling in *Nf1*-deficient cells

In light of the importance of dysregulated MAPK signaling we had seen in cell culture, we next investigated the effect of *Hsf1* loss on the MAPK/ERK pathway in tumors arising spontaneously in *NPcis* mice. All MPNSTs demonstrated comparable levels of total ERK protein but those arising in *Hsf1*-null mice had significantly lower levels of phospho-ERK compared to MPNSTs from *Hsf1*-wild type mice (Figure 5A). This finding is consistent with our previous observations, in other contexts, that HSF1 supports transformation and tumorigenesis by oncogenic *RAS* (6).

Strikingly, HSF1 supported MAPK signaling not only in *Nf1*-deficient tumors but even in primary MEFs. In the homozygous *NPcis* mutant background, primary MEFs that were *Hsf1* heterozygous or null displayed much reduced ERK phosphorylation compared to their *Hsf1* wild-type counterparts (Figure 5B). Reduced MAPK signaling in both tumors and primary cells that are *Hsf1*-deficient demonstrates a critical role for HSF1 in supporting activity of the RAS/MAPK pathway. Taken together with data from Figure 2, we propose that loss of *Nf1* activates HSF1 at least in part via activation of the MAPK/ERK pathway and that HSF1, in turn, is necessary to support MAPK signaling.

HSF1 is activated in *NF1*-deficient human tumors

Results in mouse models do not always reflect the pathophysiology of human disease. Does a

pathobiology comparable to that seen in *NPcis* mouse model operate in humans? To address this question, we first examined HSF1 activation status in a panel of five human cell lines derived from patients clinically diagnosed with Neurofibromatosis Type I. These lines express Schwann cell markers such as S100β and p75 neurotrophin receptor, consistent with Schwann cell origin (31). Three cell lines (sNF96.2, 90-8TL and S462) were devoid of neurofibromin, consistent with their reported *NF1* mutation status (32-34). Despite their clinical derivation, however, two of the lines, sNF02.2 and sNF94.3, express full-length neurofibromin protein (32, 35, 36 and Figure 6A). While the specific *NF1* mutation(s) in these two cell lines remain unknown despite sequencing of multiple exons, their elevated RAS-GTP levels suggest some impairment of neurofibromin function (37). However, these two lines exhibited significantly lower levels of activating phosphorylation of key RAS downstream effectors, C-RAF and MEK1/2 (16, 38, 39), compared to the three cell lines devoid of neurofibromin (Figure 6A). This result supports only partial loss of neurofibromin function in these two lines.

In analyzing our panel of human MPNST cells, our distinct findings clearly demonstrate that HSF1 is activated to a greater degree in those cell lines lacking neurofibromin than in those expressing neurofibromin. First, levels of HSF1 and the highly HSF1-regulated heat-shock protein HSP72 were increased (Figure 6A). Second, by immunofluorescent staining, HSF1 was increased and localized to the nucleus (Figure 6B). Third, HSF1 was robustly phosphorylated at serine residue 326 (p-S326, Figure 6A). Fourth, HSF1 was trimerized, the characteristic state of the activated protein (Figure 6C). This activation was constitutive, occurring in the absence of environmental stressors.

Furthermore, consistent with the results in *Nf1*-deficient MEFs (Figure 2, B and D), U0126 reduced Ser326 phosphorylation and nuclear translocation of HSF1 in MPNST cells (Figure 6, D and E). Thus, in human NF1 tumor cells aberrant MAPK signaling also critically regulates HSF1 activity.

Human MPNST cells are addicted to HSF1 and to MEK signaling

Do these cell lines require HSF1 to maintain their malignant phenotype? To test this, we knocked down HSF1 expression with lentiviral shRNAs. First, we tested the efficacy of different hairpins on HSF1 knockdown. As previously reported in other cell types (5), the hA6 hairpin was more effective than the hA9 hairpin in MPNST cells (Figure 7A). Suppression of HSF1 by both the hA6 and hA9 shRNAs markedly decreased cell number in lines lacking neurofibromin (Figure 7B). Moreover, transduction with hA6 caused a greater reduction than hA9, consistent with a dose-dependent effect of HSF1 on viability. As an additional control, we transduced one of the lines with low HSF1 levels that maintained neurofibromin expression with the same panel of lentiviral supernatants. Cell number was much less reduced, not only ruling out non-specific cytotoxicity as the basis for the activity of HSF1-targeted lentiviral preparations but also supporting the idea that *NF1* function is only partially compromised in sNF02.2 cells.

To provide mechanistic insight into the interplay of HSF1 and MAPK signaling in human MPNST cells, we examined the effect of HSF1 knockdown on phosphorylation of ERK, the downstream target of RAS/MAPK signaling. This endpoint had been strongly HSF1-dependent in both mouse tumors and *NPcis* MEFs (Figure 5). Compared to cells transduced with scrambled control hairpins, transduction with either hA6 or hA9 virus caused a marked decline in ERK phosphorylation, with hA6 again having the greatest effect (Figure 7C). RAS requires the scaffold protein KSR1 for efficient signaling of the MAPK/ERK pathway and KSR1 deletion inhibits RAS-driven oncogenesis (40, 41). HSF1 knockdown sharply reduced KSR1 levels in a dose-dependent manner. Because KSR1 function depends on molecular chaperones (42), the decrease in HSP72 and HSP90 levels following HSF1 knockdown (Figure 7C) could contribute to KSR1 loss. Consistent with this hypothesis, inhibition of HSP90 by geldanamycin reduced KSR1 protein levels and ERK phosphorylation in both S462 and 90-8TL cells (Figure 7D and Supplemental Figure 6A). As expected, levels of AKT, a known HSP90 client protein, were also reduced by geldanamycin.

To examine the role of KSR1 in maintaining the malignant phenotype of human MPNST cells, we transiently transfected a non-targeting and three independent KSR1-targeting siRNAs into S462 cells. In these cells, knock down of KSR1 induced apoptosis, indicated by elevated levels of cleaved PARP and Caspase 7 (Figure 7E), and reduced cell number (Figure 7F). Overall, the data support a model in which, HSF1 enables the malignant phenotype of neurofibromin-deficient cells at least in part by stabilizing KSR1 and supporting dysregulated MAPK signaling.

MEK kinase provides an attractive therapeutic target for human cancers. To examine the effects of MEK inhibition on human MPNST cells, S462 cells were treated with either U0126 or CI-1040, the first MEK inhibitor to enter clinical trials (43). Prolonged MEK inhibition over the course of several days markedly reduced the protein levels of HSF1, HSP90α, and KSR1 (Figure 8, A and B). Consistent with our observation that inhibiting MEK reconstitutes polyubiquitination of HSF1 (Figure 2I), enhanced HSF1 polyubiquitination was seen in S462 cells following overnight exposure to U0126 or CI-1040 (Figure 8C).

We also examined whether MEK inhibition reduced the cell number of human MPNST cells. Two neurofibromin-expressing MPNST cell lines and a normal diploid fibroblast control cell line were relatively resistant to MEK inhibition with CI-1040. However, two of the three neurofibromin-deficient cell lines displayed enhanced sensitivity to CI-1040 treatment (Figure 8D). Why the third line, 90-8TL was relatively insensitive is unknown, but warrants further investigation. Previous reports suggest a number of factors could be involved including mutations in *BRAF* and *PI3KCA* (44, 45).

Next we asked whether enhanced HSF1 function is sufficient to augment MAPK signaling. We generated isogenic S462 cells stably overexpressing HSF1 by viral transduction. Compared to cells stably transduced with LacZ gene, cells with HSF1 overexpression showed higher levels of KSR1 and

phospho-ERK (Figure 8E). This result was also reproduced in HEK293 cells and immortalized MEFs (Supplemental Figure 6, B and C). As expected, the levels of HSP90α and HSP72 were increased in these HSF1-overexpressing cells. These data, together with the role we have demonstrated for HSF1 in supporting MAPK signaling, establish HSF1 as an important modulator of the RAS/MAPK signaling axis. Such a feed-forward loop could enable a powerful shift in the survival landscape that facilitates tumorigenesis (Figure 8F).

HSF1 is over-expressed and activated in MPNSTs resected from patients

To move from laboratory models to clinical material, we used both immunofluorescence (IF) and immunohistochemistry (IHC) to examine HSF1 levels and localization in a panel of ten human MPNST surgical resections. High levels of HSF1 were found in the nuclei of tumor cells in all of the specimens examined. HSF1 levels were markedly higher in MPNST cells than in surrounding normal tissues, including nerve and perineurium (Supplemental Figure 7A). Benign neurofibroma demonstrated an intermediate level (Supplemental Figure 7B). Co-IF also clearly demonstrated high HSF1 levels in MPNST cells but very low levels in the infiltrated nerve (Figure 9A). Consistent with our findings in mice (Figure 5) and cultured human tumor cells (Figure 6), we detected activation-associated phosphorylation of ERK at much higher levels in HSF1-overexpressing MPNST cells than nerve (Supplemental Figure 8). Intermediate levels of phospho-ERK were observed in benign neurofibroma (Supplemental Figure 8).

In one specimen, we captured an MPNST developing from a neurofibroma; it is uncommon to observe a truly high-grade MPNST adjacent to its low-grade counterpart in an individual microscopic specimen. This opportune sample allowed us to visualize levels of HSF1 and assess its phosphorylation status during tumor progression. Captured side by side, HSF1 staining was indeed present in the nuclei of many cells in the neurofibroma but there was more intense staining for HSF1 protein in the nuclei of MPNST cells (Figure 9B and Supplemental Figure 7A and B). While p-S326

HSF1 (p-HSF1) levels were heterogeneous in benign neurofibroma cells, levels were markedly higher and uniformly expressed in the MPNST cells consistent with increasing activation of HSF1 during tumor progression (Figure 9B).

Discussion

HSF1, the master regulator of the heat-shock response in eukaryotes, is a powerful modifier of carcinogenesis (5-8). How HSF1 is activated in tumors, however, has been largely unknown. Though heat-shock proteins were known to be elevated in cancer, this was commonly ascribed to a classic "heat-shock response" in reaction to the environmental and proteomic stresses that are inherent to the malignant state. Here we report the surprising finding that HSF1 is activated by a simple genetic alteration that underlies, but precedes malignancy, loss of the *Nf1* tumor suppressor. Upon loss of *Nf1* function, dysregulated MAPK signaling engages HSF1. In turn, HSF1 supports and further augments activation of the MAPK pathway to drive tumorigenesis. This feed-forward loop arises from intrinsic genetic alteration, not from environmental stress. Activation of HSF1 in this fashion allows cells to withstand a range of proteotoxic insults even during very early stages of tumorigenesis, thereby enabling the process. The same pathobiology is at work in NF1-associated malignancies in human patients where activation of HSF1 arises in neurofibroma and more robust and uniform activation of HSF1 then occurs during progression to MPNST.

A new mode of HSF1 activation: Tumor suppressor loss

During tumorigenesis, micro-environmental challenges such as nutrient deprivation and hypoxia (46) and cell-autonomous challenges such as genomic instability, altered metabolism, reactive oxygen species and the burden of mutated and misfolded oncoproteins must all be successfully managed by malignant cells to permit their survival (47, 48). These stresses, inherent to malignant transformation, progression, and metastasis are made tolerable by a range of innate adaptive responses. The HSF1-mediated response is one of several critical systems that make adaptation not only possible but efficient. Other responses mediated by regulators such as Hypoxia-Inducible Factor 1 (HIF1), Nuclear factor kappa B (NFκB) and Stress-activated Protein Kinases, (p38 MAPK and JNK) participate as well to enable cancer cells to adapt and prosper (49-51).

Understanding how stress response regulators are engaged during malignant transformation is of both basic interest and potential therapeutic value. In the case of HSF1, the drivers of activation, the point in tumorigenesis when this occurs, and the functional consequences have remained poorly defined. The stimulus most widely assigned to drive HSF1 activation in cancer is increased substrate burden on the heat-shock protein/chaperone machinery. Dysregulation of the protein translation machinery (52), imbalanced protein production due to aneuploidy (53,54) and accumulation of mutated, highly chaperone-dependent oncoproteins all strain the chaperone machinery (55-57). Support for this model of HSF1 activation comes from observations that the HSP90-based chaperone machinery may be pressed to operate at its maximal capacity in cancer cells (58), thereby releasing HSF1 from a repressive complex with HSP90 (59).

Alongside this model of HSF1 activation, we now describe another driver for HSF1 activation, loss of the tumor suppressor *Nf1.* Not only does HSF1 accumulate in the nucleus of neurofibromin deficient cells but total levels of HSF1 protein and activating phosphorylation of HSF1 all increase. This indicates a role for the HSF1-adaptive response even in the earliest phases of tumorigenesis, when dysplasia and pre-malignant alterations begin to arise. By coordinating the diverse biological processes required for tumorigenesis, HSF1 can play a critical role in providing a permissive cellular environment that cultivates the very inception of a neoplasm. Interestingly, in a recent study in breast cancer we observed that HSF1 is frequently activated in developing neoplasms prior to invasion while the tumor cells still remain in situ (60). Our findings in *Nf1* null cells now suggest that HSF1 can be at work even earlier in tumorigenesis, before atypical changes in cell morphology become visually evident.

Although *NF1* was cloned almost 2 decades ago (61), our understanding of exactly how neurofibromin impacts growth, metabolism and survival to act as a key tumor suppressor remains incomplete. The findings reported here further expand our understanding of this tumor suppressor, revealing a previously unrecognized function for *NF1* in modulating the cellular response to proteotoxic

stress. The tumor suppressor *NF1* prevents activation of the heat-shock response under basal conditions by restraining improper activation of the MAPK signaling. Upon *NF1* loss, however, dysregulated MAPK signaling induces HSF1 phosphorylation, nuclear translocation and an increase in the level of HSF1 protein through impaired proteasomal degradation.

Dysregulated MAPK signaling is important for HSF1 activation during tumor development, supporting a relationship between tumorigenesis and HSF1 activation that is deeply rooted in the molecular biology and signaling aberrations of *NF1*-associated tumorigenesis, not solely in environmental and proteotoxic triggers. The importance of MAPK signaling in HSF1 recruitment suggests that other mitogenic pathways dysregulated by dominantly acting oncogenes may also impact HSF1 activity (55). The question now arises: Is loss of other classical tumor suppressors such as *p53, RB* or *PTEN* alone sufficient to activate HSF1? It seems likely that it is a combination of many factors that evoke the robust activation of HSF1 observed in very high-grade tumors, compared to the more modest activation seen in their lower-grade counterparts from which they often develop.

HSF1 shapes the tumor landscape

What are the functional consequences of HSF1 activation? These are only beginning to emerge. Here, we found that *Nf1* loss leads to an HSF1-dependent capacity to tolerate a broad range of proteotoxic perturbations. The chemical stressors we employed likely phenocopy some of the internal proteomic imbalances as well as the environmental pressures that tumors must accommodate during their initiation and progression. By fostering an ability to thrive in unfavorable conditions, HSF1 ultimately can promote enhanced malignant behavior. Indeed, in a separate study of over 1,800 women with invasive breast cancer from the Nurses' Health Study we recently found that HSF1 activation is associated with tumor size, histologic grade and likelihood of metastasis (60). This work demonstrates that HSF1 is an independent predictor of poor outcome in breast cancer (60). These strong epidemiological associations implicating HSF1 in malignancy are supported here by knockdown

experiments demonstrating a direct and critical role for HSF1 in promoting the viability of MPNST cells lines derived from advanced cancers.

In addition to facilitating survival under stress, HSF1 also supports tumor growth through its integral role in a feed-forward loop supporting the pro-proliferative MAPK pathway. Not only is HSF1 activated by MAPK signaling but its activation, in turn, robustly supports increased flux through this signaling axis both in MEF and in MPNST cells. By supporting this particular signaling pathway, which is central to the pathophysiology of NF1, HSF1 alters the NF1 phenotype, as suggested by our observation of a shift in tumor spectrum and latency. How it might impact other features of clinical NF1 such as neurodevelopmental abnormalities would be fascinating to investigate. Lastly, important as MAPK signaling may be, the impact of HSF1 on NF1-associated malignancies undoubtedly extends beyond effects on this one signaling pathway and is likely rooted in the compendium of diverse cellular processes that HSF1 uniquely regulates in tumors.

HSF1 as a therapeutic target in NF1?

The critical dependence of established MPNST cell lines on HSF1, the expression of HSF1 at high levels in surgical resection specimens and its activation-associated phosphorylation firmly establish the importance of HSF1 in enabling NF1-associated tumorigenesis in humans. Targeting HSF1 could represent a new way of approaching anti-cancer therapy. Non-genotoxic strategies would be particularly important in NF1 because patients are at markedly increased risk of developing treatment-related myeloid leukemias after exposure to conventional alkylating agents (62). Moreover, our finding that HSF1 expression and activation are associated with malignant potential and outcome in breast cancer (60) suggests that HSF1 status should be evaluated as a potential novel prognostic marker for human NF1 malignancies, particularly MPNSTs.

Is HSF1 a plausible therapeutic target? Genetic knockout of *Hsf1* is sufficient to completely abrogate induction of the heat-shock response following temperature shift. Normal basal expression of

the major heat-shock protein classes is preserved, however, which makes HSF1 dispensable for growth and survival of mammalian cells under physiological conditions. Indeed knockout mice deficient for *Hsf1* develop essentially normally and prosper under non-stress conditions (19, 63). This feature and our finding that even haploinsufficiency of *Hsf1* impairs tumorigenesis suggest that a useful therapeutic index for selective inhibitors of HSF1 is likely to exist.

Unfortunately, no small, drug-like inhibitors of the heat-shock response have yet been identified that target HSF1 in a convincingly specific manner. Most, if not all appear to act on the cascade of post-translational modifications mediated by kinases, phosphatases, acetylases and conjugating enzymes involved in regulating HSF1 activation (64, 65). Discovery efforts are in their infancy, however, with great potential for further progress (64-67).

Many important questions remain, but the findings reported here provide a deeper basic understanding of how cellular physiology accommodates constitutive loss of *NF1* function. The adaptive HSF1 program set in motion enhances cell survival but comes at the cost of enabling tumor formation in this common cancer predisposition syndrome. Likely a similar phenomenon occurs in sporadic human cancers driven by other tumor suppressor abnormalities or even mutant oncogenes.

Methods

Cells, tissues and reagents

See Supplemental Experimental Methods for details.

Real time quantitative RT-PCR:

Total RNAs were extracted using a USB PrepEase RNA Spin Kit (Affymetrix). 100ng RNAs were used for reverse transcription using a Maxima First Strand cDNA Synthesis kit (Fermentas). Equal amounts of cDNA were used for quantitative RCR reaction using Maxima SYBR Green/ROX qPCR Master Mix (Fermentas). Signals were detected by an ABI 7500 Real-Time PCR System (Applied Biosystems). The sequences of individual primers for each gene are listed in the Supplemental Materials.

Transfection and luciferase reporter assay:

Plasmids were transfected into HEK293T cells with Arrest-In™ transfection reagent (Open Biosystems). The following plasmids were used in transfection experiments: pBabe-EGFP (generated from pEGFP-N3 plasmid), pBabe–MEK1^{AA} (generated by site-directed mutagenesis), pHSE-firefly luciferase (Clontech), pCMV-renilla luciferase (Promega), and pBabe-HSF1 (Addgene#1948). Luciferase activities were quantitated using a Promega Dual-Glo® Luciferase Assay System using a VICTOR^3 Multilabel plate reader (PerkinElmer).

Tumorigenesis studies in *NPcis* mice

NPcis mice (129/Sv) were generously provided by Karen Cichowski (Brigham and Women's Hospital, Boston, Massachusetts, USA). Mice (C57BL/6) heterozygous for disruption of the *Nf1* gene were generously provided by Karlyne Reilly (National Cancer Institute, Frederick, Maryland, USA). Mice were crossed to *Hsf1*-modified mice (mixed 129/SvJ and Balb/cJ), a gift from Ivor Benjamin (28, University of Utah, Salt Lake City, Utah, USA). Moribund mice or mice with severely compromised body condition were euthanized, a full necropsy was performed, and all major tissues were harvested and fixed in 10%

formalin (soft tissues) or Bouin's fixative (bone). Incidental tumors were documented in the spectrum of tumors depicted in Supplemental Fig.3B but were not included in the assessment of tumor free-survival (Fig. 4A). Tumors were identified and diagnosed in consultation with Roderick Bronson (Tufts University, Boston, Massachusetts, USA).

Proliferation and survival assays

Relative cell growth and survival was measured in 96-well microplate format using the fluorescent detection of resazurin dye reduction as an endpoint. Proliferation of primary MEF was measured following a five-day exposure to the indicated compounds.

Immunoblotting and Immunoprecipitation

Whole-cell protein extracts were prepared in cold lysis buffer (100 mM NaCl, 30 mM Tris-HCl pH 7.6, 1% NP-40, 30 mM sodium fluoride, 1 mM EDTA, 1 mM sodium orthovanadate, and protease inhibitor cocktail tablet from Roche Diagnostics). Proteins were separated on SDS-PAGE gels and transferred to nitrocellulose membranes. Primary antibodies were applied in wash buffer for 1 hr at room temperature or overnight at 4^0C. Peroxidase-conjugated secondary antibodies were applied at room temperature for 1 hr and signal visualized by chemiluminescent substrate (Thermo-Fisher Scientific) followed by exposure to film.

For immunoprecipitation, 500µg of whole cell lysates were incubated with either 4µg rat monoclonal HSF1 antibodies (Thermo-Fisher Scientific, RT-629-PABX) or normal rat IgG overnight at 4^0C. Then, 50 µl of protein G magnetic beads (GenScript) were added for 1hr at RT. After 3 times of washing with PBS, beads were boiled in 50µl sample loading buffer for 5 min before loading on SDS-PAGE.

Immunostaining of cells and tissues

Archival clinical specimens and mouse tissues were processed as formalin-fixed, paraffin-embedded tissue blocks. Serial 4 µm sections were cut for hematoxylin and eosin staining and immunostaining. Detection of NFP (Monosan, clone: 2F11, 1:900), phospho-ERK (Cell Signaling Technology, #4370, 1:500) and phospho-HSF1 (Epitomics #2092-1, 1:1200) was achieved by immunohistochemistry. Deparaffinized sections were blocked with 3% H_2O_2 and antigen retrieval was achieved using a pressure cooker with Dako citrate buffer (pH6.0) at 120ºC +/- 2ºC, 15 +/- 5 PSI. Primary antibodies were incubated on sections at room temperature for 40 min followed by 30 min incubation with Dako Labeled Polymer-HRP IgG as a secondary antibody. Immunoreactivity was visualized with 3,3'-diaminobenzidine (Dako Envision+ System). For HSF1 immunostaining, rat monoclonal antibodies (1:1000) were used with the ABC method. Slides were blocked with 3% normal rabbit serum. Biotinylated rabbit anti-rat was applied as secondary antibody (Vector Labs, BA-4000) and detection was achieved by 30 min incubation with Vectastain Elite ABC reagent (Vector Labs, PK-6100). Mayer hematoxylin was used for counterstaining. For immunofluorescent staining, reactivity was visualized with secondary anti-IgG antibodies labeled with either Cy3 or Cy5. Primary antibody dilutions were anti-HSF1 (1:250), and anti-NFP (1:300). 4',6-diamidino-2-phenylindole (DAPI, 0.5 µg/ml) was applied to visualize cell nuclei.

Statistical methods

All statistical analyses were performed using Prism 5.0 (GraphPad software). Statistical significance cut-off for all comparisons: $p \leq 0.05$.

Study approval

Paraffin blocks of human surgical resection specimens were obtained from an archive maintained by the Department of Pathology, Brigham and Women's Hospital under an IRB-approved excess tissue protocol. Ethics committee review specifically waived the need for informed consent. All mouse experiments were performed under a protocol approved by the MIT Animal Care and Use Committee.

Acknowledgements:

We thank S. Silver and D. Root of the Broad Institute RNAi platform for assisting in the design and execution of the shRNA screening experiments. We thank A. W. Cheng and E. Yeger-Lotem for assistance in selecting heat-shock related genes for shRNA targeting. M. Topolski and M. Koeva provided expert technical assistance while members of the Lindquist laboratory provided many helpful comments.

S.L. is a senior investigator of the Howard Hughes Medical Institute. S.S is supported by NIH grant K08NS064168, and grants from the Valvano Foundation, the American Brain Tumor Association and the Brain Science Foundation. This work was supported in part by the USAMRMC Neurofibromatosis Research Program (SL), the Johnson & Johnson COSAT program (LW), the Marble Fund (SS/SL), the Children's Tumor Foundation and NIH grant 1DP2OD007070 (C.D).

References

1. Ahn SG, Thiele DJ. Redox regulation of mammalian heat shock factor 1 is essential for Hsp gene activation and protection from stress. *Genes Dev.* 2003;17(4):516-528.

2. Voellmy R. On mechanisms that control heat shock transcription factor activity in metazoan cells. *Cell Stress Chaperones.* 2004;9(2):122-133.

3. Trinklein ND, Murray JI, Hartman SJ, Botstein D, Myers RM. The role of heat shock transcription factor 1 in the genome-wide regulation of the mammalian heat shock response. *Mol Biol Cell.* 2004;15(3):1254-1261.

4. Balch WE, Morimoto RI, Dillin A, Kelly JW. Adapting proteostasis for disease intervention. *Science.* 2008;319(5865):916-919.

5. Dai C, Whitesell L, Rogers AB, Lindquist S. Heat shock factor 1 is a powerful multifaceted modifier of carcinogenesis. *Cell.* 2007;130(6):1005-1018.

6. Min JN, Huang L, Zimonjic DB, Moskophidis D, Mivechi NF. Selective suppression of lymphomas by functional loss of Hsf1 in a p53-deficient mouse model for spontaneous tumors. *Oncogene.* 2007;26(35):5086-5097.

7. Jin X, Moskophidis D, Mivechi NF. Heat shock transcription factor 1 is a key determinant of HCC development by regulating hepatic steatosis and metabolic syndrome. *Cell Metab.* 2011;14(1):91-103.

8. Scott KL, et al. Proinvasion metastasis drivers in early-stage melanoma are oncogenes. *Cancer Cell.* 2011;20(1):92-103.

9. Bollag G, et al. Loss of NF1 results in activation of the Ras signaling pathway and leads to aberrant growth in haematopoietic cells. *Nat Genet.* 1996;12(2):144-148.

10. Cichowski K, Jacks T. NF1 tumor suppressor gene function: narrowing the GAP. *Cell.* 2001;104(4):593-604.

11. Largaespada DA, Brannan CI, Jenkins NA, Copeland NG. Nf1 deficiency causes Ras-mediated granulocyte/macrophage colony stimulating factor hypersensitivity and chronic myeloid leukaemia. *Nat*

Genet. 1996;12(2):137-143.

12. Gutmann DH, Boguski M, Marchuk D, Wigler M, Collins FS, Ballester R. Analysis of the neurofibromatosis type 1 (NF1) GAP-related domain by site-directed mutagenesis. *Oncogene.* 1993;8(3):761-769.

13. Tanaka K, et al. S. cerevisiae genes IRA1 and IRA2 encode proteins that may be functionally equivalent to mammalian ras GTPase activating protein. *Cell.* 1990;60(5):803-807.

14. Turbyville TJ, et al. Search for Hsp90 inhibitors with potential anticancer activity: isolation and SAR studies of radicicol and monocillin I from two plant-associated fungi of the Sonoran desert. *J Nat Prod.* 2006;69(2):178-184.

15. Guettouche T, Boellmann F, Lane WS, Voellmy R. Analysis of phosphorylation of human heat shock factor 1 in cells experiencing a stress. *BMC Biochem.* 2005;6:4.

16. Zheng CF, Guan KL. Activation of MEK family kinases requires phosphorylation of two conserved Ser/Thr residues. EMBO J. 1994;13(5):1123-1131.

17. Nalepa G, Rolfe M, Harper JW. Drug discovery in the ubiquitin-proteasome system. Nat Rev Drug Discov. 2006;5(7):596-613.

18. Gitler AD, Epstein JA. Regulating heart development: the role of Nf1. *Cell Cycle.* 2003;2(2):96-98.

19. Xiao X, et al. HSF1 is required for extra-embryonic development, postnatal growth and protection during inflammatory responses in mice. *EMBO J.* 1999;18:5943-5952.

20. Xu YM, et al. 2,3-Dihydrowithaferin A-3beta-O-sulfate, a new potential prodrug of withaferin A from aeroponically grown Withania somnifera. *Bioorg Med Chem.* 2009;17(6):2210-2214.

21. Santagata S, et al. Using the Heat-Shock Response To Discover Anticancer Compounds that Target Protein Homeostasis. ACS Chem Biol. 2011; Epub ahead of print. DOI: 10.1021/cb200353m.

22. Gitler AD, et al. Nf1 has an essential role in endothelial cells. *Nat Genet.* 2003;33(1):75-79.

23. Jacks T, Shih TS, Schmitt EM, Bronson RT, Bernards A, Weinberg RA. Tumour predisposition in mice heterozygous for a targeted mutation in Nf1. *Nat Genet.* 1994;7(3):353-361.

24. Cichowski K, et al. Mouse models of tumor development in neurofibromatosis type 1. *Science.* 1999;286(5447):2172-2176.

25. Vogel KS, Klesse LJ, Velasco-Miguel S, Meyers K, Rushing EJ, Parada LF. Mouse tumor model for neurofibromatosis type 1. *Science.* 1999;286(5447):2176-2179.

26. Hsu AL, Murphy CT, Kenyon C. Regulation of aging and age-related disease by DAF-16 and heat-shock factor. *Science.* 2003;300(5622):1142-1145.

27. Morley JF, Morimoto RI. Regulation of longevity in Caenorhabditis elegans by heat shock factor and molecular chaperones. *Mol Biol Cell.* 2004;15(2):657-664.

28. Steele AD, et al. Heat shock factor 1 regulates lifespan as distinct from disease onset in prion disease. *Proc Natl Acad Sci U S A.* 2008;105(36):13626-13631.

29. Reilly KM, et al. An imprinted locus epistatically influences Nstr1 and Nstr2 to control resistance to nerve sheath tumors in a neurofibromatosis type 1 mouse model. Cancer Res. 2006;66(1):62-68.

30. Walrath JC, Fox K, Truffer E, Gregory Alvord W, Quinones OA, Reilly KM. Chr 19(A/J) modifies tumor resistance in a sex- and parent-of-origin-specific manner. Mamm Genome. 2009;20(4):214-223.

31. Zhu Y, Ghosh P, Charnay P, Burns DK, Parada LF. Neurofibromas in NF1: Schwann cell origin and role of tumor environment. *Science.* 2002;296(5569):920-922.

32. Fieber LA, Gonzalez DM, Wallace MR, Muir D. Delayed rectifier K currents in NF1 Schwann cells. Pharmacological block inhibits proliferation. *Neurobiol Dis.* 2003;13(2):136-146.

33. Frahm S, et al. Genetic and phenotypic characterization of tumor cells derived from malignant peripheral nerve sheath tumors of neurofibromatosis type 1 patients. *Neurobiol Dis.* 2004;16(1):85-91.

34. Barkan B, Starinsky S, Friedman E, Stein R, Kloog Y. The Ras inhibitor farnesylthiosalicylic acid as a potential therapy for neurofibromatosis type 1. *Clin Cancer Res.* 2006;12(18):5533-5542.

35. Li Y, et al. Notch and Schwann cell transformation. *Oncogene.* 2004;23(5):1146-1152.

36. Miller SJ, et al. Integrative genomic analyses of neurofibromatosis tumours identify SOX9 as a

biomarker and survival gene. *EMBO Mol Med.* 2009;1(4):236-248.

37. Perrin GQ, et al. Plexiform-like neurofibromas develop in the mouse by intraneural xenograft of an NF1 tumor-derived Schwann cell line. *J Neurosci Res.* 2007;85(6):1347-1357.

38. Diaz B, Barnard D, Filson A, MacDonald S, King A, Marshall M. Phosphorylation of Raf-1 serine 338-serine 339 is an essential regulatory event for Ras-dependent activation and biological signaling. Mol Cell Biol. 1997;17(8):4509-4516.

39. Alessi DR, et al. Identification of the sites in MAP kinase kinase-1 phosphorylated by p74raf-1. EMBO J. 1994;13(7):1610-1619.

40. Therrien M, Michaud NR, Rubin GM, Morrison DK. KSR modulates signal propagation within the MAPK cascade. *Genes Dev.* 1996;10(21):2684-2695.

41. Kortum RL, Lewis RE. The molecular scaffold KSR1 regulates the proliferative and oncogenic potential of cells. *Mol Cell Biol.* 2004;24(10):4407-4416.

42. Stewart S, Sundaram M, Zhang Y, Lee J, Han M, Guan KL. Kinase suppressor of Ras forms a multiprotein signaling complex and modulates MEK localization. *Mol Cell Biol.* 1999;19(8):5523-5534.

43. Allen LF, Sebolt-Leopold J, Meyer MB. CI-1040 (PD184352), a targeted signal transduction inhibitor of MEK (MAPKK). Semin Oncol. 2003;30(5 Suppl 16):105-116.

44. Corcoran RB, Dias-Santagata D, Bergethon K, Iafrate AJ, Settleman J, Engelman JA. BRAF gene amplification can promote acquired resistance to MEK inhibitors in cancer cells harboring the BRAF V600E mutation. Sci Signal.3(149):ra84.

45. Wee S, et al. PI3K pathway activation mediates resistance to MEK inhibitors in KRAS mutant cancers. Cancer Res. 2009;69(10):4286-4293.

46. Fang JS, Gillies RD, Gatenby RA. Adaptation to hypoxia and acidosis in carcinogenesis and tumor progression. *Semin Cancer Biol.* 2008;18(5):330-337.

47. Luo J, Solimini NL, Elledge SJ. Principles of cancer therapy: oncogene and non-oncogene addiction. *Cell.* 2009;136(5):823-837.

48. Vander Heiden MG, Cantley LC, Thompson CB. Understanding the Warburg effect: the metabolic

requirements of cell proliferation. *Science.* 2009;324(5930):1029-1033.

49. Ono K, Han J. The p38 signal transduction pathway: activation and function. *Cell Signal.* 2000;12(1):1-13.

50. Karin M. NF-kappaB as a critical link between inflammation and cancer. *Cold Spring Harb Perspect Biol.* 2009;1(5):a000141.

51. Semenza GL. Defining the role of hypoxia-inducible factor 1 in cancer biology and therapeutics. *Oncogene.* 2010;29(5):625-634.

52. Cencic R, et al. Reversing chemoresistance by small molecule inhibition of the translation initiation complex eIF4F. *Proc Natl Acad Sci U S A.* 2011;108(3):1046-1051.

53. Wang Y, Theriault JR, He H, Gong J, Calderwood SK. Expression of a dominant negative heat shock factor-1 construct inhibits aneuploidy in prostate carcinoma cells. *J Biol Chem.* 2004;279(31):32651-32659.

54. Pavelka N, et al. Aneuploidy confers quantitative proteome changes and phenotypic variation in budding yeast. *Nature.* 2010;468(7321):321-325.

55. Khaleque MA, et al. Induction of heat shock proteins by heregulin beta1 leads to protection from apoptosis and anchorage-independent growth. *Oncogene.* 2005;24(43):6564-6573.

56. Whitesell L, Lindquist SL. HSP90 and the chaperoning of cancer. *Nat Rev Cancer.* 2005;5(10):761-772.

57. Stanhill A, et al. Ha-ras(val12) induces HSP70b transcription via the HSE/HSF1 system, but HSP70b expression is suppressed in Ha-ras(val12)-transformed cells. *Oncogene.* 2006;25(10):1485-1495.

58. Kamal A, et al. A high-affinity conformation of Hsp90 confers tumour selectivity on Hsp90 inhibitors. *Nature.* 2003;425(6956):407-410.

59. Voellmy R, Boellmann F. Chaperone regulation of the heat shock protein response. *Adv Exp Med Biol.* 2007;594:89-99.

60. Santagata S, et al. High levels of nuclear heat-shock factor 1 (HSF1) are associated with poor prognosis in breast cancer. *Proc Natl Acad Sci U S A.* 2011;108(45):18378-18383.

61. Li Y, et al. Somatic mutations in the neurofibromatosis 1 gene in human tumors. *Cell.* 1992;69(2):275-

281.

62. Chao RC, et al. Therapy-induced malignant neoplasms in Nf1 mutant mice. *Cancer Cell.* 2005;8(4):337-348.

63. McMillan DR, Xiao X, Shao L, Graves K, Benjamin IJ. Targeted disruption of heat shock transcription factor 1 abolishes thermotolerance and protection against heat-inducible apoptosis. *J. Biol. Chem.* 1998;273(13):7523-7528.

64. Whitesell L, Lindquist S. Inhibiting the transcription factor HSF1 as an anticancer strategy. *Expert Opin Ther Targets.* 2009;13(4):469-478.

65. Akerfelt M, Morimoto RI, Sistonen L. Heat shock factors: integrators of cell stress, development and lifespan. *Nat Rev Mol Cell Biol.* 2011;(8):545-555.

66. Au Q, Zhang Y, Barber JR, Ng SC, Zhang B. Identification of inhibitors of HSF1 functional activity by high-content target-based screening. *J. Biomol. Screen.* 2009;14(10):1165-1175.

67. Yoon YJ, et al. KRIBB11 inhibits HSP70 synthesis through inhibition of heat shock factor 1 function by impairing the recruitment of positive transcription elongation factor b to the hsp70 promoter. *J Biol Chem.* 2011;286(3):1737-1747.

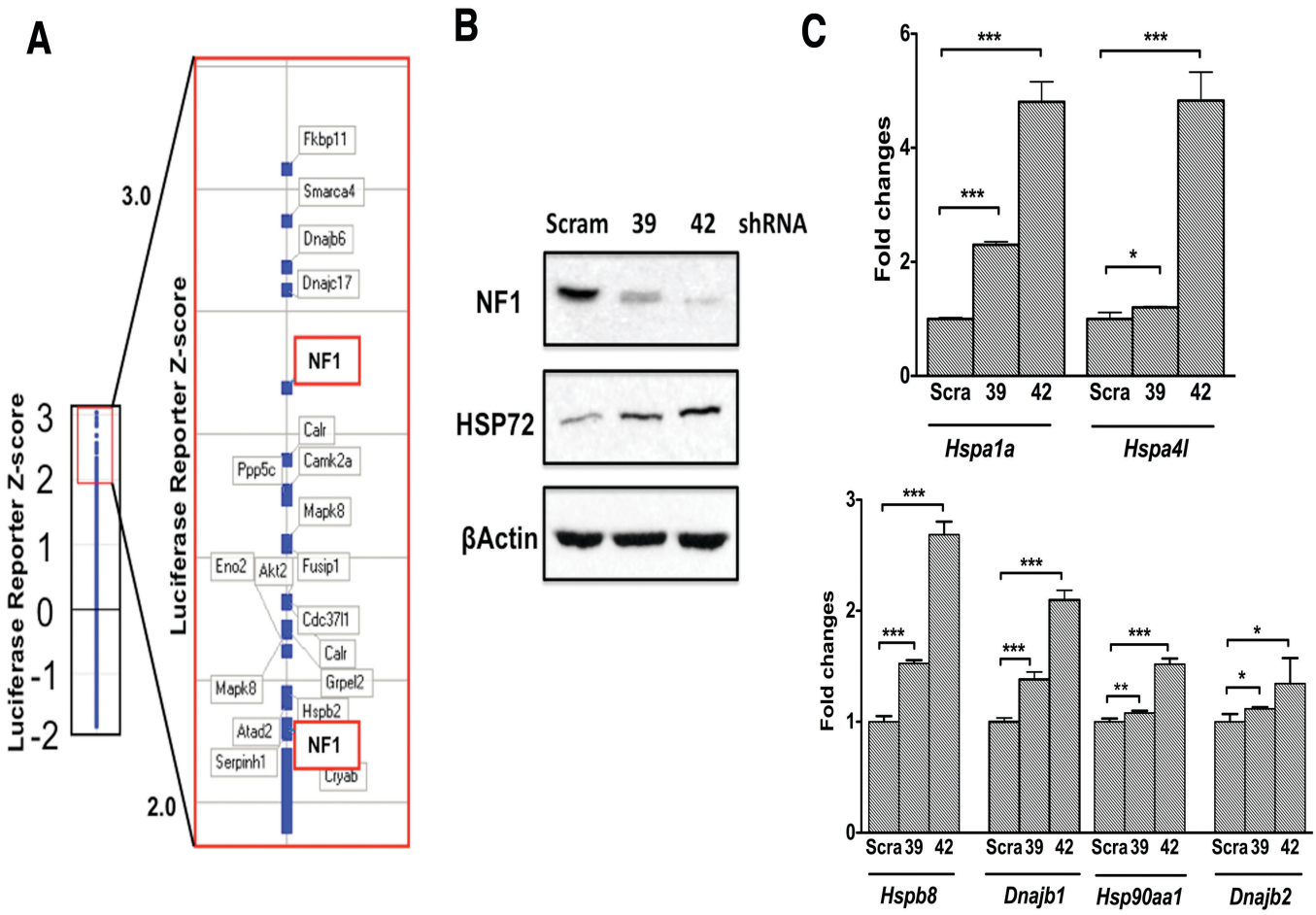

Figure 1. Genetic compromise of NF1 induces the heat-shock response. (**A**) Whole cell-based screen of a heat shock-oriented shRNA library. Heat-shock reporter NIH3T3 cells arrayed in 384-well format were infected with lentiviral constructs designed to target 175 candidate genes. Five days later, reporter activation was measured by luciferase assay. The mean Z-score calculated from 2 biological replicates for each construct is plotted as a measure of activation relative to the entire population of wells that were assayed. Two independent *Nf1*-targeted hairpins that strongly activate the heat-shock reporter are highlighted in bold. (**B**) *Nf1* knockdown increases HSP72 expression in an immortalized MEF cell line. MEFs were stably transduced with two shRNAs (#39 and #42) that target different regions of the *Nf1* mRNA and a scrambled control shRNA. Neurofibromin (NF1) and HSP72 protein levels were examined by immunoblotting. (**C**) *Nf1* knockdown transcriptionally activates the heat-shock response. Transcript levels of chaperones in *Nf1*-knockdown MEFs were measured by two-step qRT-PCR technique. Transcript levels relative to cells transduced with a scrambled control shRNA for each of the indicated genes were expressed as fold changes (mean±SD, n=3 or 4, Student's t-test, * $p<0.05$; ** $p<0.01$; *** $p<0.001$).

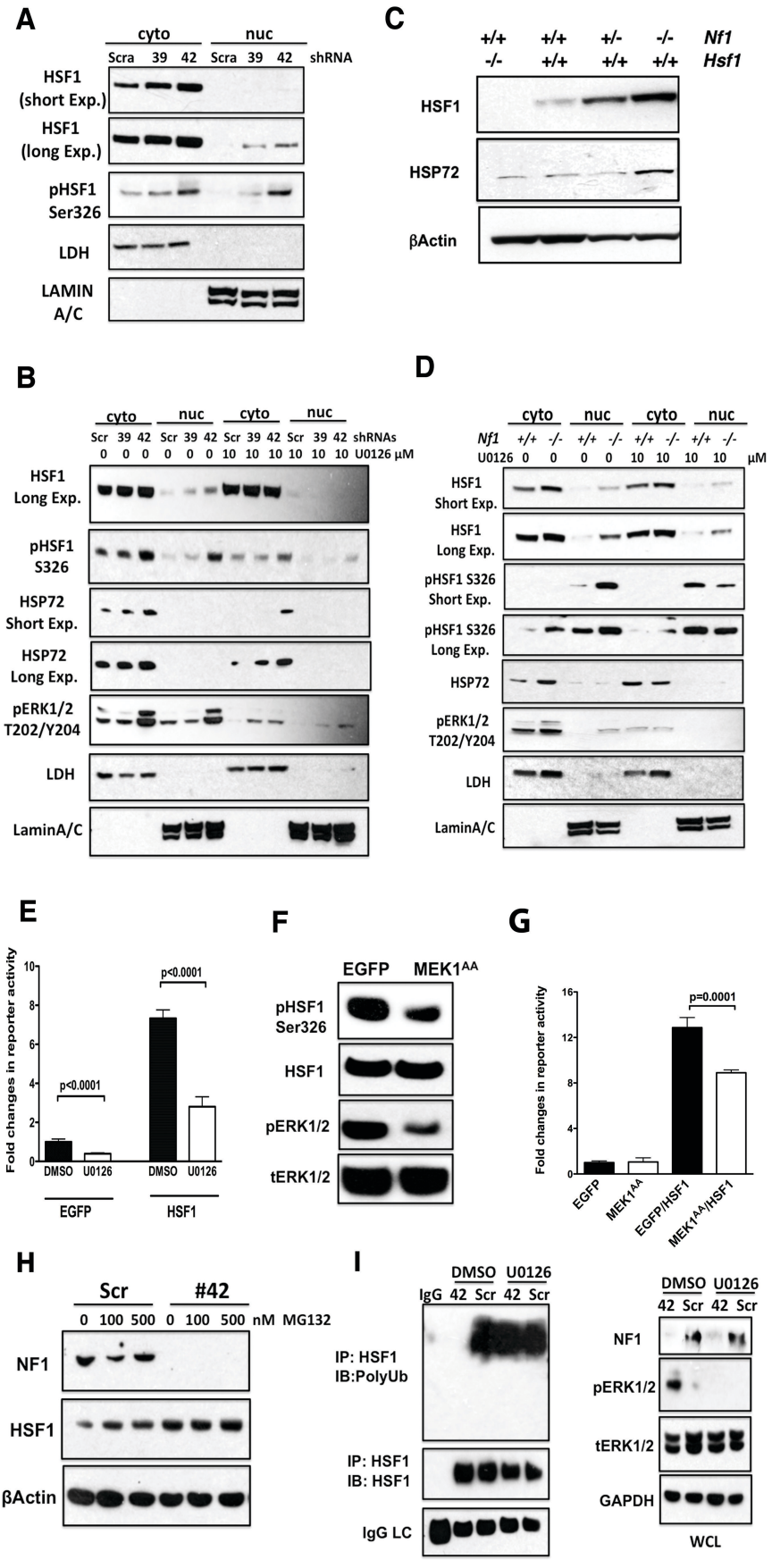

Figure 2: NF1 loss activates HSF1 via elevated MAPK signaling. (**A** and **B**) *Nf1* knockdown activates HSF1. Cytoplasmic and nuclear fractions were prepared from immortalized MEFs following overnight treatment of DMSO or 10μM U0126. Blotting for cytoplasmic lactate dehydrogenase (LDH) and nuclear Lamins A/C confirms appropriate fractionation. (**C** and **D**) HSF1 is activated in primary *Nf1*-knockout MEFs. (**E**) MEK inhibition impairs HSF1 transcriptional activity. EGFP or -HSF1 plasmids were transfected with pHSE-firefly luciferase reporter plasmid and pCMV-renilla luciferase plasmid into HEK293T cells. After 1 day cells were treated with either DMSO or 20μM U0126 overnight. Firefly luciferase signals were normalized against renilla luciferase signals (mean±SD, n=6, Student's t-test). (**F**) Dominant negative MEK1 impairs HSF1 Ser326 phosphorylation. EGFP or –$MEK1^{AA}$ plasmids were transfected into HEK293T cells and after 3 days cells were harvested for immunoblotting. (**G**) Dominant negative MEK1 impairs HSF1 transcriptional activity. In HEK293T cells, EGFP or –$MEK1^{AA}$ plasmid was transfected with the luciferase reporter plasmids. Further, HSF1 plasmid was co-transfected with either EGFP or –$MEK1^{AA}$ plasmid. Three days after transfection, luciferase signals were measured (mean±SD, n=4, Student's t-test). (**H**) Proteasomal inhibition leads to accumulation of HSF1 protein. MEFs were treated with DMSO or MG132 overnight. (**I**) HSF1 polyubiquitination is suppressed in *Nf1*-knockdown cells and re-established following MEK inhibition. MEFs were treated with either DMSO or 20μM U0126 overnight and whole cell lysates were immunoprecipitated for HSF1. Normal rat IgG served as the control. Precipitates were immunoblotted for polyubiquitinated conjugates and HSF1. LC: light chain; WLC: whole cell lysates.

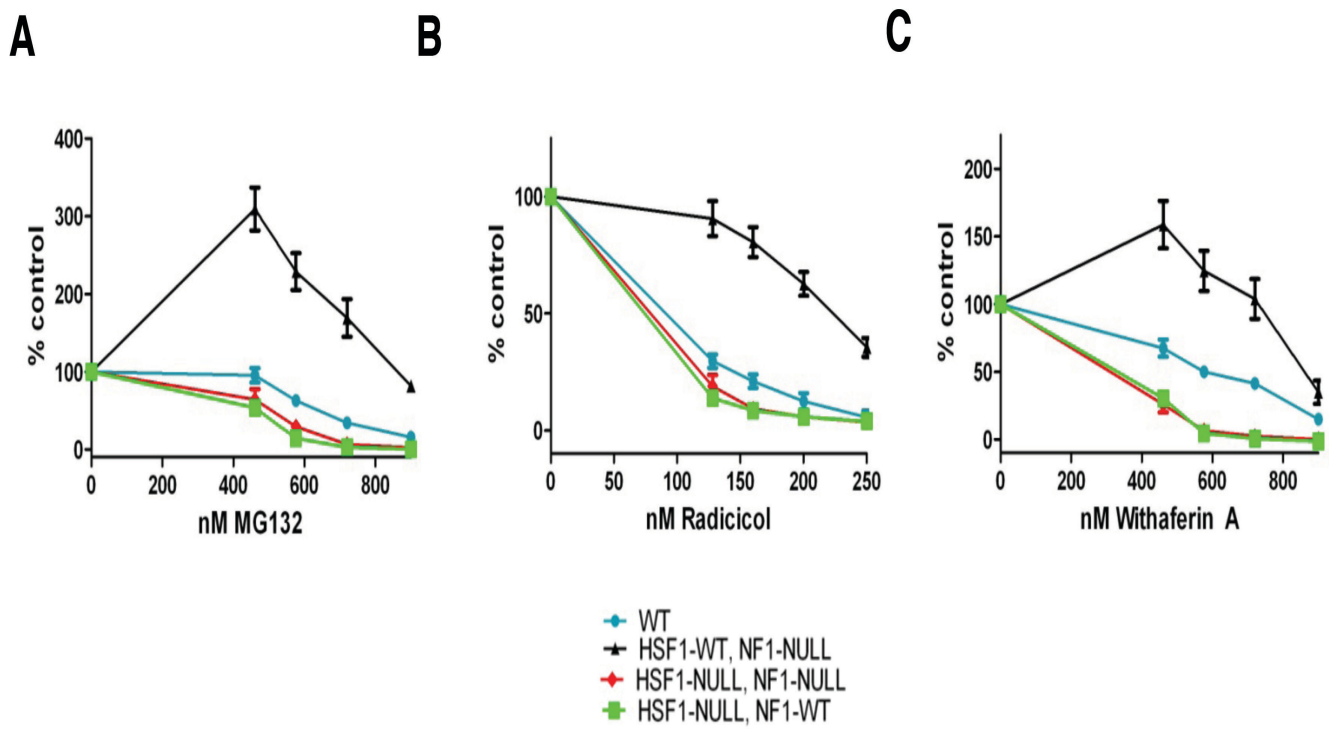

Figure 3: HSF1 activation by *Nf1* knockout renders cells resistant to proteotoxic stress. Primary MEFs of the indicated genotypes were plated at low density (2,000 cells per well) and exposed for 5 days to the indicated concentrations of (**A**) MG132, (**B**) Radicicol and (**C**) Withaferin A. Resazurin dye reduction was assayed as a measure of relative viable cell number. The mean of triplicate determinations repeated in two separate experiments is presented. (mean±SD. ***p<.001, two-way ANOVA).

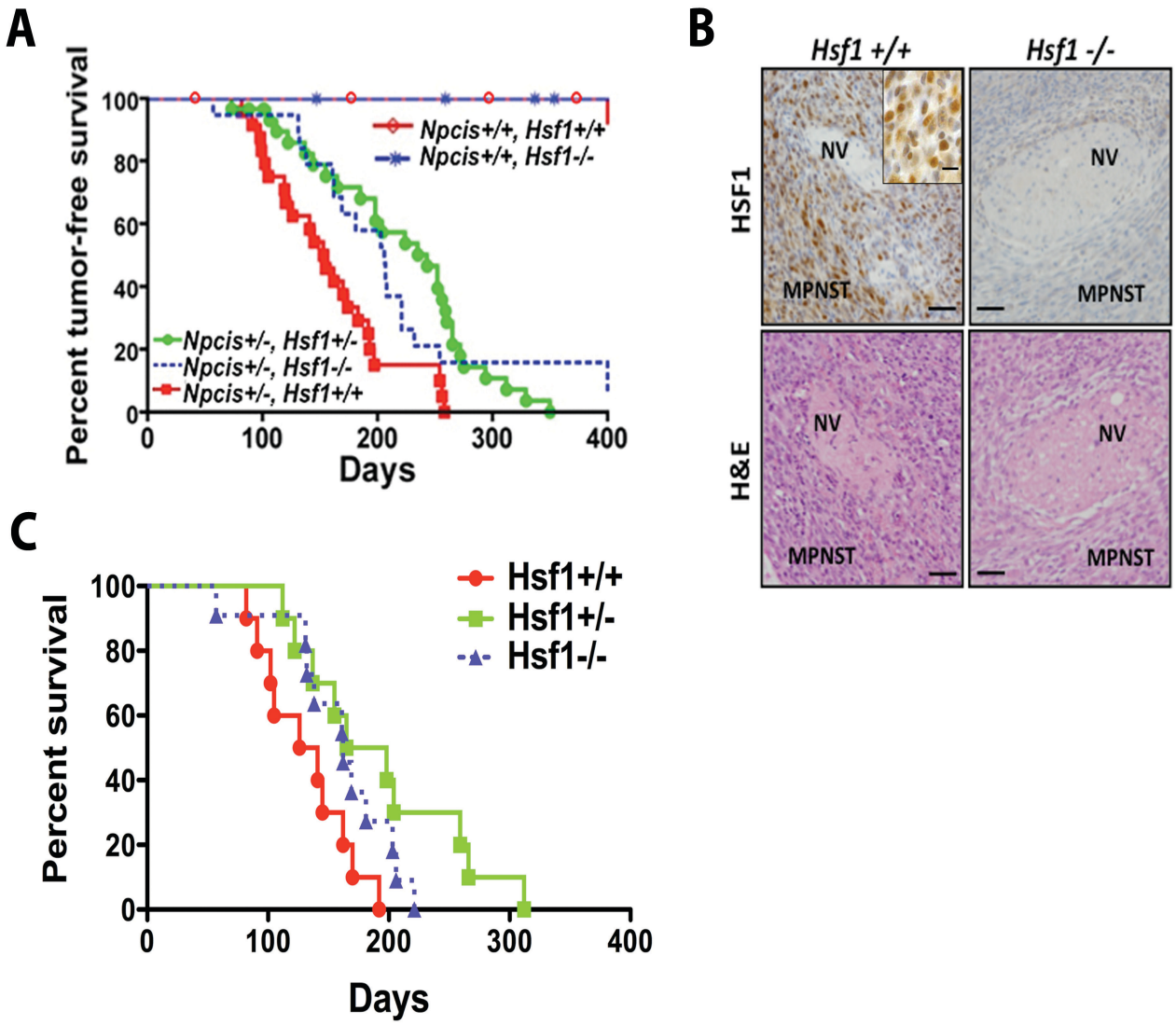

Figure 4. Genetic compromise of *Hsf1* prolongs survival in a mouse model of NF1. (**A**) Tumor occurrence is suppressed in *NPcis* mice when *Hsf1* is disrupted. Tumor-free survival in relationship to *Hsf1* genotype is plotted for Control (*NPcis +/+)* and *NPcis* transgenic (*NPcis* +/-) mice. Median survival for *NPcis* mice: *Hsf1* +/+ 22 weeks (n=24), *Hsf1* +/- 34 weeks (n=30, *Hsf1* +/+ vs +/- p=0.0002, Logrank test), *Hsf1 -/-* 29 weeks (n=19, *Hsf1* +/+ vs -/- p=0.028, Log-rank test). (**B**) Representative micrographs of serial sections from MPNSTs arising in *NPcis* mice were immunostained for HSF1 to reveal increased levels in tumor but not adjacent normal nerve (NV). Scale bar: 100 μm..The inset shows nuclear HSF1 staining in tumors (scale bar: 10 μm). Lower panels were stained with hematoxylin and eosin (H&E) to demonstrate histology and provide orientation. (**C**) Survival time of *NPcis* mice that developed MPNST only is prolonged by *Hsf1* compromise. Median survivals: *Hsf1*+/+ 19 weeks, *Hsf1*+/- 23.5 weeks (*Hsf1* +/+ vs +/- p=0.0152, Logrank test), *Hsf1-/-* 23 weeks (*Hsf1* +/+ vs -/- p=0.0869, Log-rank test).

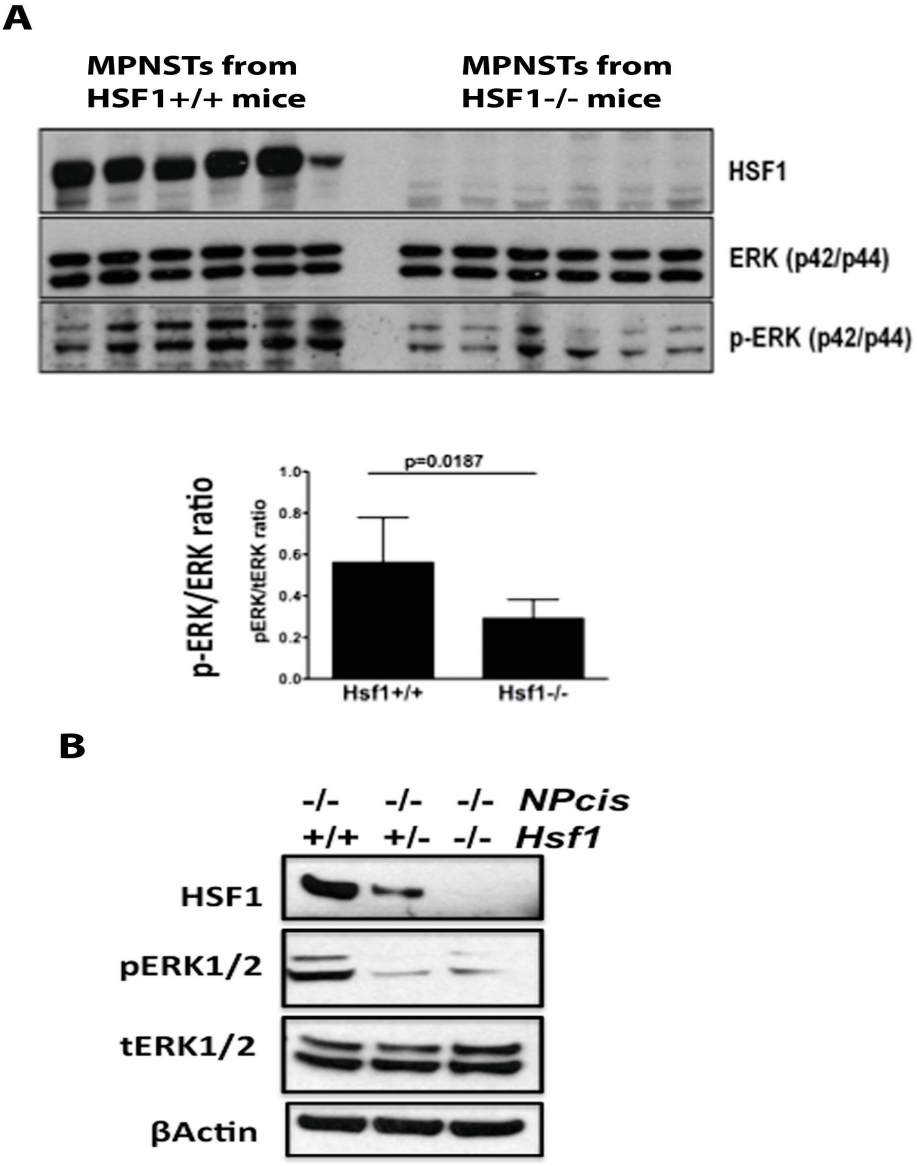

Figure 5. *Hsf1*-deficiency attenuates MAPK signaling in *NPcis* mice. (**A**) *Upper:* Immunoblotting demonstrates equivalent levels of total ERK, but less activation-associated phosphorylation (p-ERK) in MPNSTs arising in *Hsf1* null mice. *Lower:* Densitometric quantitation of immunoblots confirms statistically significant difference in mean ratio of p-ERK to total ERK (student's t-test). (**B**) Basal phosphorylation of ERK is diminished in *NPcis-/-* MEFs derived from *Hsf1* heterozygous and null embryos.

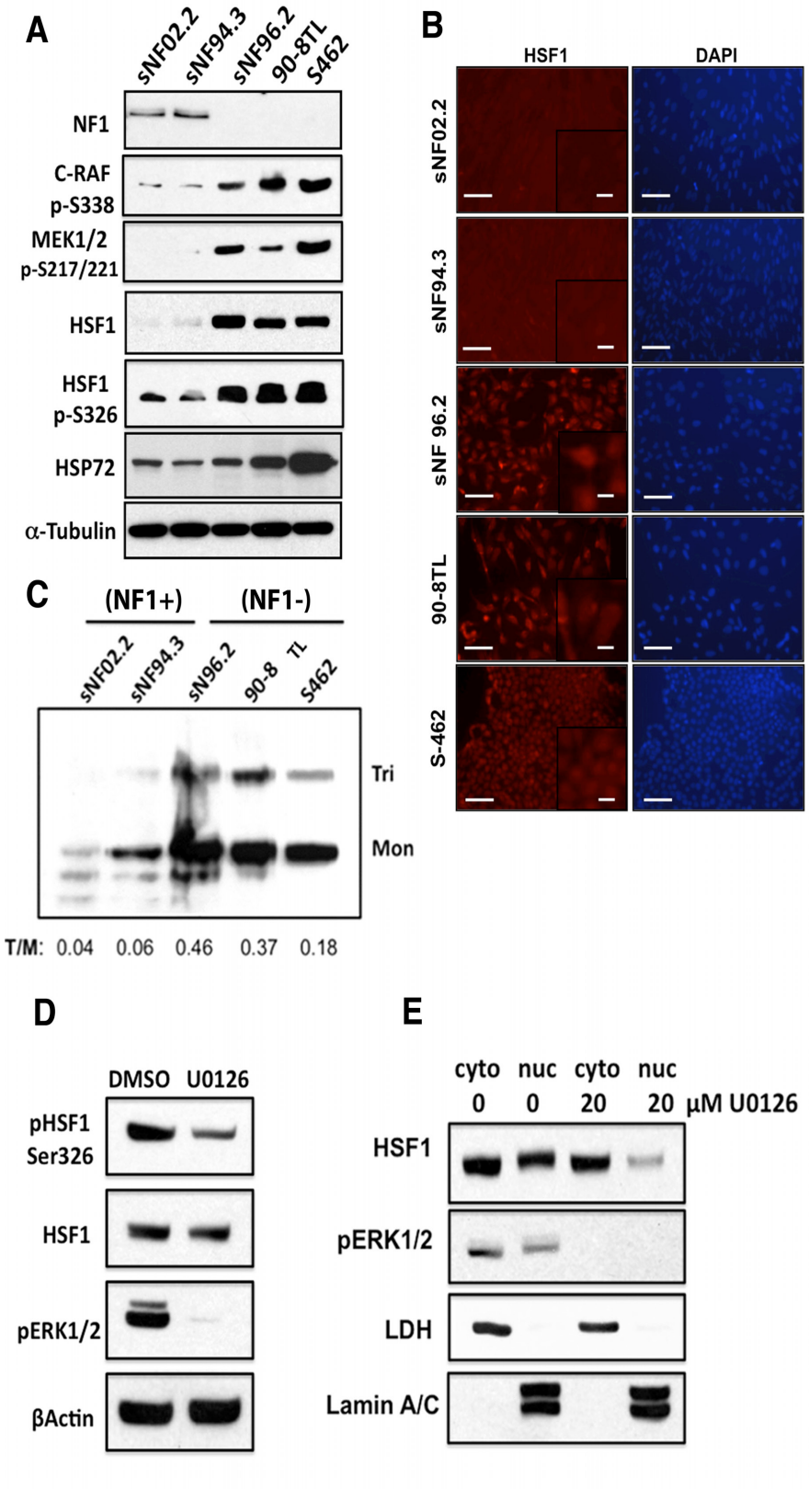

Figure 6. HSF1 is overexpressed and activated in human MPNST cell lines lacking neurofibromin. (**A**) Immunoblotting of cell lines with complete loss of neurofibromin show elevated phospho-C-RAF, phospho-MEK1/2, total and phospho-HSF1 as well as HSP72 levels in comparison to lines that maintain full-length neurofibromin expression. (**B**) Immunofluorescent staining confirms HSF1 overexpression in cells without neurofibromin (scale bar: 25 μm). The insets illustrate nuclear HSF1 staining (scale bar: 5 μm). DAPI counterstaining is presented to visualize cell nuclei (right panels). All images were acquired at identical magnification. (**C**) Immunoblotting of cross-linked cell lysates demonstrates an increase in activation-associated trimeric (Tri) versus inactive monomeric (Mon) forms of HSF1 in MPNST cells without neurofibromin (NF1-) compared to lysates from NF1+ cell lines. The Tri/Mon ratio (T/M) in lysates as measured by densitometry is indicated. (**D**) and (**E**) MEK inhibition reduces HSF1 Ser326 phosphorylation and nuclear translocation in human MPNST cells. S462 cells were treated with 20μM U0126 overnight. Total pHSF1 Ser326 and nuclear HSF1 were detected by immunoblotting.

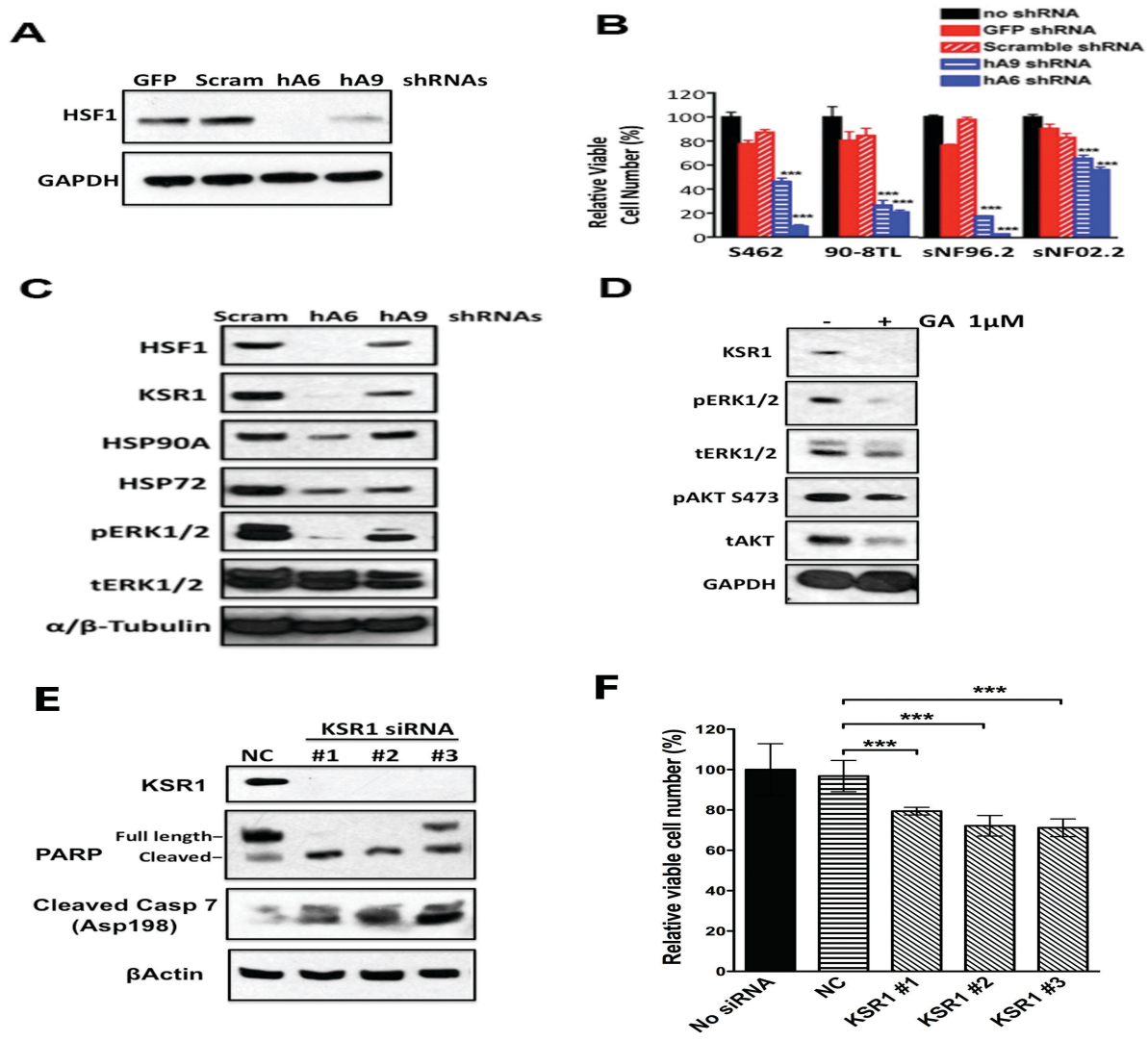

Figure 7: HSF1 knockdown impairs the growth of human MPNST cells and attenuates MAPK signaling. (**A**) Differential efficacy of HSF1-targeting shRNA constructs. S462 cells were transduced with control (GFP, Scram) or HSF1-targeting (hA9, hA6) lentiviral supernatants and harvested for immunoblotting. (**B**) HSF1 knockdown impairs net growth and survival of MPNST cells. After plating, cells were transduced with viral supernatants as indicated. Relative viable cell number in each well was measured 4 days after viral transduction by resazurin dye reduction assay. Raw fluorescence data were normalized to values obtained in wells that underwent mock transduction (mean±SD, n =5, ***p<0.001, two-way ANOVA). (**C**) Decreased levels of KSR1, phospho-ERK, HSP90α and HSP72 following HSF1 knockdown. S462 cells were stably transduced with the indicated viral supernatants and harvested for immunoblotting. (**D**) Decreased levels of KSR1 and phospho-ERK following HSP90 inhibition. S462 cells were treated overnight with 1μM geldanamycin and harvested for immunoblotting. (**E**) KSR1 knockdown induces apoptosis in MPNST cells. S462 cells were transfected with either a non-targeting siRNA (NC) or 3 independent KSR1-targeting siRNAs (#1, 2, and 3) at 25nM final concentration. Two days after transfection, cells were harvested for immunoblotting. (**F**) KSR1 knockdown impairs net growth and survival of MPNSTs. S462 cells plated in 96-well format were transiently transfected without or with 25nM siRNAs. Relative viable cell number in each well was measured as described in (B) 3 days after transfection (mean±SD, n =5, ***p<0.001, one-way ANOVA).

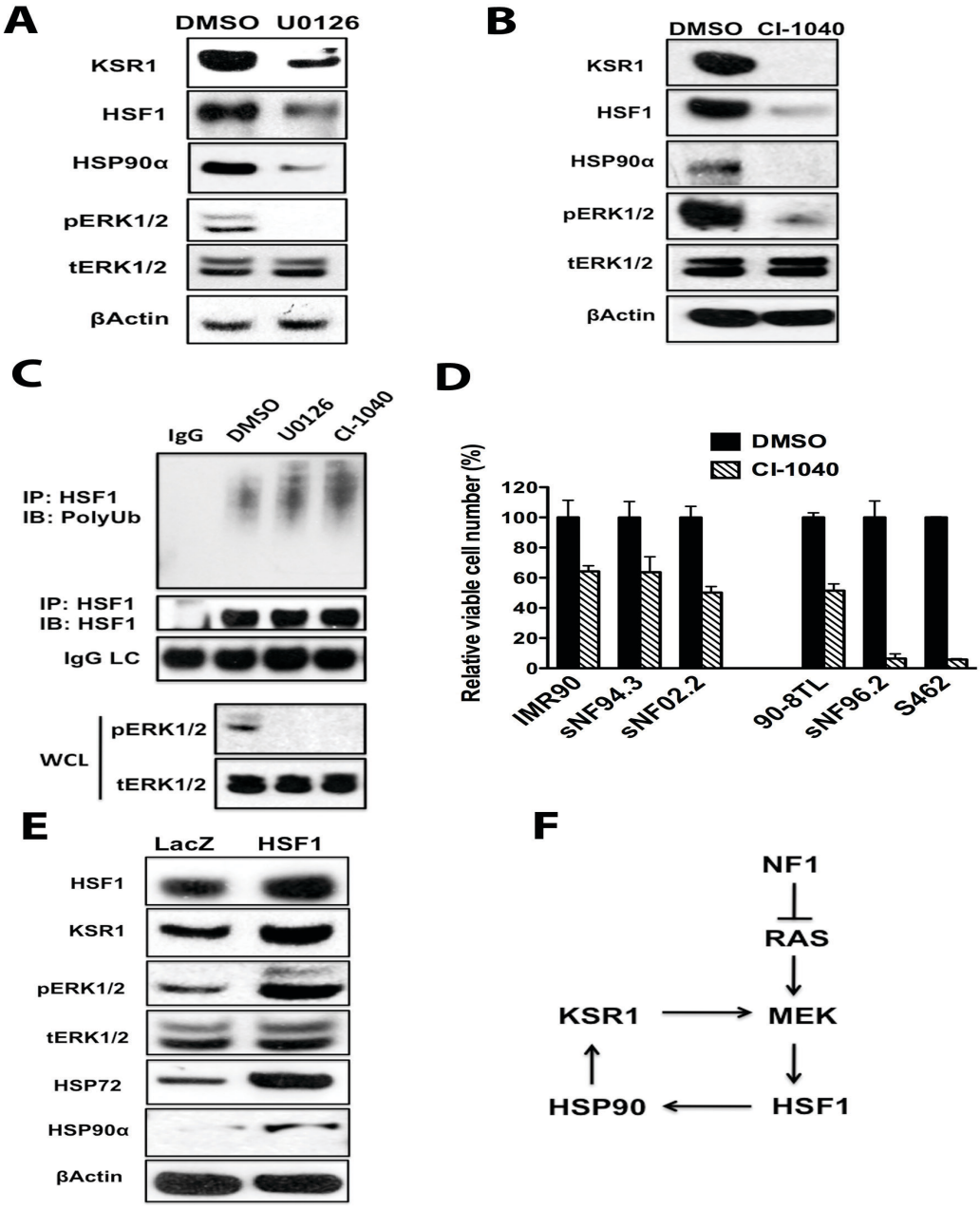

Figure 8: A feed-forward loop of MEK/HSF1. (**A** and **B**) Prolonged MEK inhibition decreases HSF1, HSP90α, and KSR1 protein levels in MPNST cells. S462 cells were treated with 20μM U0126 for 4 days or 20μM CI-1040 for 3 days. Whole cell lysates were subjected to immunoblotting. (**C**) MEK inhibition enhances HSF1 polyubiquitination. S462 cells were treated with 20μM U0126 or CI-1040 overnight. HSF1 polyubiquitination was detected as described in Fig. 2I. (**D**) MEK inhibition impairs net growth and survival of MPNST cells. MPNST cells were plated in 96-well format (2000 cells/well) and treated with DMSO or 20μM CI-1040 for 4 days. Relative viable cell number in each well was measured (mean±SD, n =3). (**E**) HSF1 overexpression increases HSP90α and KSR1 protein levels and enhances ERK phosphorylation. S462 cells were transduced with lentiviral LacZ or HSF1 particles. After stable selection with blasticidin, cells were harvested for immunoblotting. (**F**) The proposed feed-forward loop of MEK/HSF1.

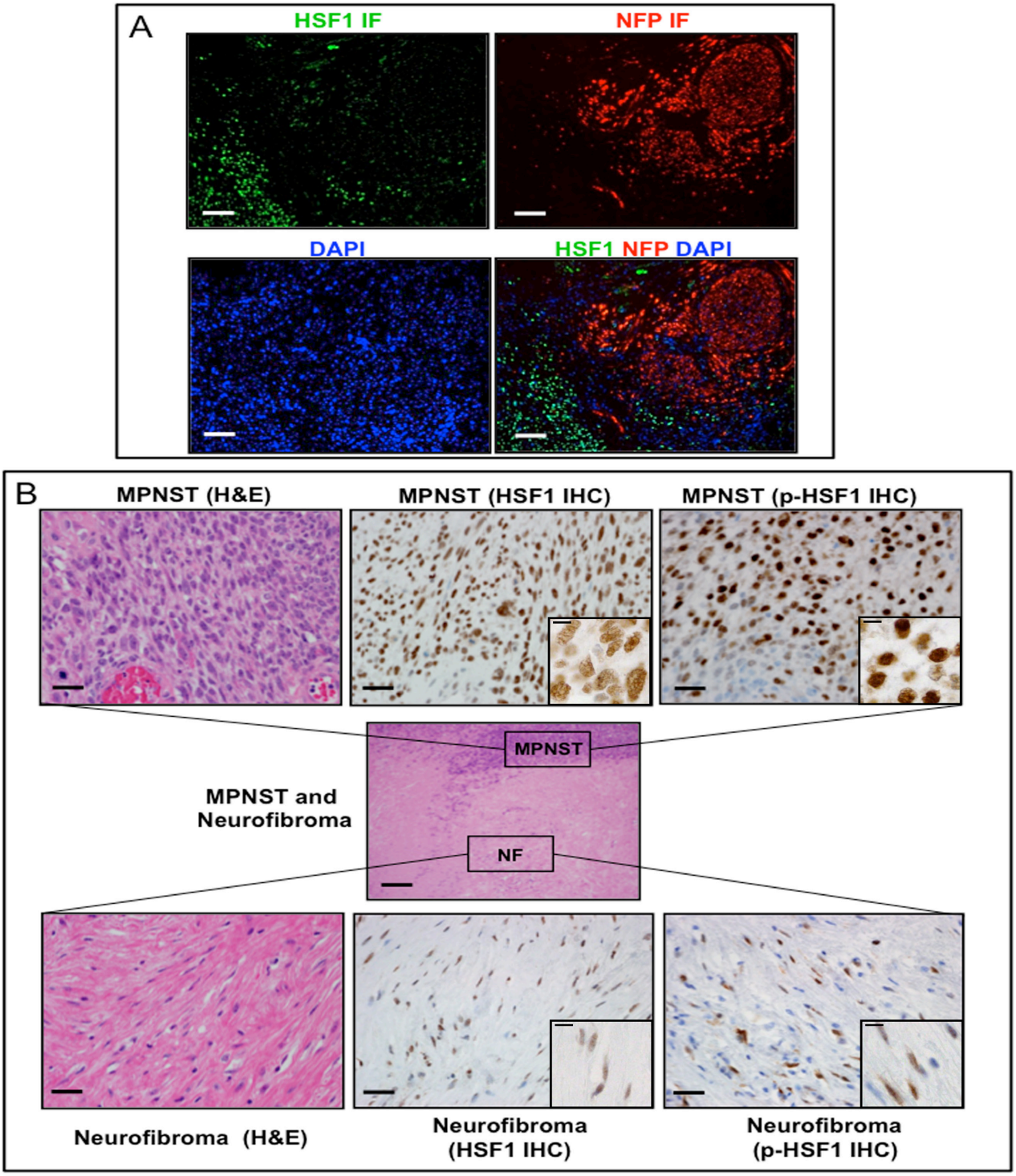

Figure 9: HSF1 is overexpressed and activated in NF1 patient tumor resections. (**A**) Photomicrographs of dual immunofluorescent staining for HSF1 (green signal) and Neurofilament protein (red signal). DAPI counterstaining was used to visualize cell nuclei (blue signal). Scale bar: 25 µm. (**B**) Photomicrographs of immunohistochemical (IHC) staining for HSF1 and phospho-HSF1 (p-HSF1) in a surgical specimen that captures an MPNST arising from adjacent neurofibroma. Brown signal depicts immunoreactivity. Pale blue counterstaining is provided by Mayer hematoxylin. Higher magnification images: scale bar, 25 µm; Inset images: scale bar, 10 µm; Lower magnification central image: scale bar, 250 µm.

Supplemental materials comprised of 8 figures, their legends, 2 tables, and additional experimental methods.

Itemized list of figures and their relevance to manuscript

Supplemental Figure 1: Supports statements in the text about the diverse functionality of HSF1-interacting proteins and how candidate genes for shRNA knockdown were selected.

Supplemental Figure 2: Positive control experiment for HSF1 nuclear translocation following heat shock and quantitation of immunoblot in Figure 2B.

Supplemental Figure 3: In support of Figure 4, panel A presents total survival as impacted by deaths from both tumor-related and non-tumor related causes for control HSF1 mice (*NPcis* +/+, *Hsf1+/+; NPcis* +/+, *Hsf1*-/-). Panel B presents the effects of *Hsf1* compromise on the tumor spectrum of *NPcis* mice. Panel C presents a positive correlation between glioma incidence and survival time.

Supplemental Figure 4: Histological evidence that diverse tumor types arise in *NPcis* mice as claimed in the text.

Supplemental Figure 5: Supports the assertion that *Hsf1* compromise prolongs the tumor-free survival of *NPcis* mice. Panel A and B present insignificant effect of the genetic modifier *Nstr2* on the survival of *NPcis* mice. Panel C-F present insignificant effect of sex on the survival of *NPcis* mice.

Supplemental Figure 6: Supports the assertions that inhibiting HSP90 results in KSR1 destabilization in Figure 7 and that HSF1 overexpression increases the levels of KSR1 and ERK phosphorylation in Figure 8.

Supplemental Figure 7: Immunohistochemical data supporting a key conclusion in text that HSF1 is preferentially over-expressed by the malignant elements within an MPNST.

Supplemental Figure 8: Immunohistochemical evidence supporting the claim that ERK is activated to a much greater extent in MPNST cells than in normal nerve or benign neurofibroma.

Supplemental Table 1: Summary of all the *NPcis* mice included in this study.

Supplemental Table 2: Summary of D15mit111 and D19mit59 genotyping results.

Supplemental methods:

Cells, tissues and reagents

Human MPNST cell lines sNF96.2 (CRL-2884), sNF94.3 (CRL-2886) and sNF02.2 (CRL-2885) were purchased from the American Type Culture Collection (ATCC). S462 (33) and 90-8TL (34) cells were generously provided by Karen Cichowski (Brigham and Women's Hospital, Boston, Massachusetts, USA). Primary MEF cultures were established from day E13 transgenic embryos by enzymatic digestion and mechanical dissociation. All cell cultures were maintained under 5% CO2 in DMEM (ATCC) supplemented with 10% fetal bovine serum (Sigma).

Immunoblotting and immunostaining for HSF1 were performed with a cocktail of 3 rat monoclonal antibodies (Ab4, Thermo-Fisher Scientific) while phosphoserine 326 HSF1 was detected by rabbit monoclonal antibody (Epitomics). Antibodies for total ERK, phospho-ERK, cleaved PARP, cleaved Caspase 7, tubulin, and lamin A/C were from Cell Signaling Technologies. KSR1 rabbit monoclonal antibody (EPR2421Y) was from Millipore. Neurofibromin antibody was from Santa Cruz Biotechnologies. HSP90 and HSP72 antibody were from Assay Designs (SPA-810) and GAPDH from Chemicon (MAB374). Monoclonal antibody-HRP conjugate recognizing polyubiquitinylated proteins was from Enzo Life Sciences (FK2H).

U0126, Radicicol and MG132 were purchased from Sigma. Withaferin A was purchased from Chromadex. CI-1040 was purchased from Selleck Chem. Cytoplasmic and nuclear fractions were prepared using the NE-PER Nuclear protein Extraction Kit from Pierce according to manufacturer' instructions.

Heat-shock reporter cells

Reporter cells were generated by infecting NIH-3T3 cells with a lentiviral vector encoding a fusion protein consisting of enhanced GFP fused to firefly luciferase under control of *HSP70B'* promoter

elements (14). The plasmid encoding the fusion protein was generously provided by Khalid Shah (Massachusetts General Hospital, Boston, Massachusetts, USA). The recombinant reporter was packaged by co-transfection of 293T cells with pCMV-VSVG and pCMV-deltaVPR. To isolate a homogenous population of high responding cells, a transduced culture was heat shocked at 42°C for 1hr, then processed 8hrs later by fluorescence activated cell sorting (FACS). Prior to use for shRNA screening, cells were reverse selected by FACS to eliminate a minority population of cells constitutively expressing the reporter in the absence of induction.

High throughput production of lentiviral shRNA supernatants

Transfection-quality DNA encoding hairpin constructs in the pLKO.1 lentiviral backbone was prepped using 96-well PureLink kits (Invitrogen). Average yields of 4 mg DNA/well, were quantified using a Pico-Green assay (Molecular Probes), and normalized robotically in each plate. Lentiviral supernatants were made in 96-well format by transfecting packaging cells (293T) with a three-plasmid system (http://www.broad.mit.edu/genome_bio/trc/rnai.html).

Lentiviral infection of reporter cells

Screening was performed in Optimem medium (Invitrogen) supplemented with 2.5% FBS. Reporter cells were seeded at a density of 2,000 cells/well into 384-well assay plates and allowed to adhere for 24 hr prior to infection in the presence of polybrene (8 μg/ml) via robotic transfer of shRNA lentiviral supernatant (4 μl/well) from 96-well viral production plates. The following day, medium was replaced with fresh Optimem. All infections were performed in duplicate with an additional replicate performed to confirm infection efficiency by adding selection antibiotic during the medium change post infection (puromycin, 2 μg/ml). Five days post-infection relative viable cell number per well was monitored using resazurin prior to measurement of reporter induction using One-Glo luciferase assay reagent (Promega, 10 μl/well).

Primer sequences for qRT-PCR:

Primers	Sequence 5' to 3'
Ms_HSPA1A-F	ATGGACAAGGCGCAGATCC
Ms_HSPA1A-R	CTCCGACTTGTCCCCCAT
Ms_HSP10-F	AGTTTCTTCCGCTCTTTGACAG
Ms_HSP10-R	TGCCACCTTTGGTTACAGTTTC
Ms_Dnajb1-F	TTCGACCGCTATGGAGAGGAA
Ms_Dnajb1-R	CACCGAAGAACTCAGCAAACA
Ms_Dnajb2-F	ACCACACGCAGAATCATGGAG
Ms_Dnajb2-R	CTAGTGCCAGGTCATCTGGGA
Ms_Hspb8-F	TCCCGTGCTCCTACCCAAG
Ms_Hspb8-R	GCTGTCAAGTCGTCTGGAAAAG
Ms_HspA4L-F	TTCCTCAACTGCTACATCGCT
Ms_HspA4L-R	AATTGCCCAGTTAATGTCCTTGA
Ms_Hsp90AA1-F	AATTGCCCAGTTAATGTCCTTGA
Ms_Hsp90AA1-F	CGTCCGATGAATTGGAGATGAG

Primer sequences for SSLP genotyping:

Primers	Sequence 5' to 3'
D15mit111-F	GTTTCAGAAGGCAATGTCTGG
D15mit111-R	GCTCAGTGCTAATCTCTGACTCC
D19mit59-F	CTCTAACTATCCTCTGACCTTCACA
D19mit59-R	TTTTAAGCAGAACATTGAGGACC

Lentiviral shRNA knockdown

Lentiviral shRNA plasmids targeting mouse *Nf1* (NM_010897) and human *Hsf1* (NM_005526) were obtained from the Broad Institute RNAi platform and are deposited in the Open Biosystems collection under the following TRCID numbers (bold font indicates text references used for each plasmid): Nf1:TRCN0000034339, and TRCN0000034342; HSF1:TRCN0000007480 (**hA6**), TRCN0000007483 (**hA9**). Control hairpins targeting **GFP** (5'-GCAAGCTGACCCTGAAGTTCA-3') and a scrambled

sequence with no known homology to any human gene (**Scram**; 5'-CCTAAGGTTAAGTCGCCCTCG-3') have been described previously (5).

HSF1 trimer cross-linking:

Equal amounts of extracted nuclear proteins were incubated with 1mM EGS (ethylene glycol bis[succinimidylsuccinate] (Thermo-Fisher Scientific) at RT for 30 min and the reactions were quenched by 50mM glycine for 15 min. The cross-linked proteins were subjected to SDS-PAGE and immunoblotted for HSF1.

siRNA Knockdown

KSR1-targeting siRNAs and a non-targeting siRNA were ordered from Dharmacon. siRNAs were transiently transfected into cells at 25nM final concentration using Lipofectamine® RNAiMAX reagent following the instructions (Invitrogen).

Simple sequence length polymorphism (SSLP) genotyping

Genomic DNAs were extracted from frozen tumor tissues or mouse tails. Regular PCR was applied to genotype *Nstr1* (D19mit59 marker) and *Nstr2* (D15mit111 marker) loci. PCR products were separated on 3% agarose gels. Genomic DNAs derived from inbred 129/SvJ or Babl/cJ mice (The Jackson Laboratory DNA Resource) were used to serve as positive controls.

Image densitometry

All digital western blotting images were quantitated by the free software package ImageJ according to the instructions.

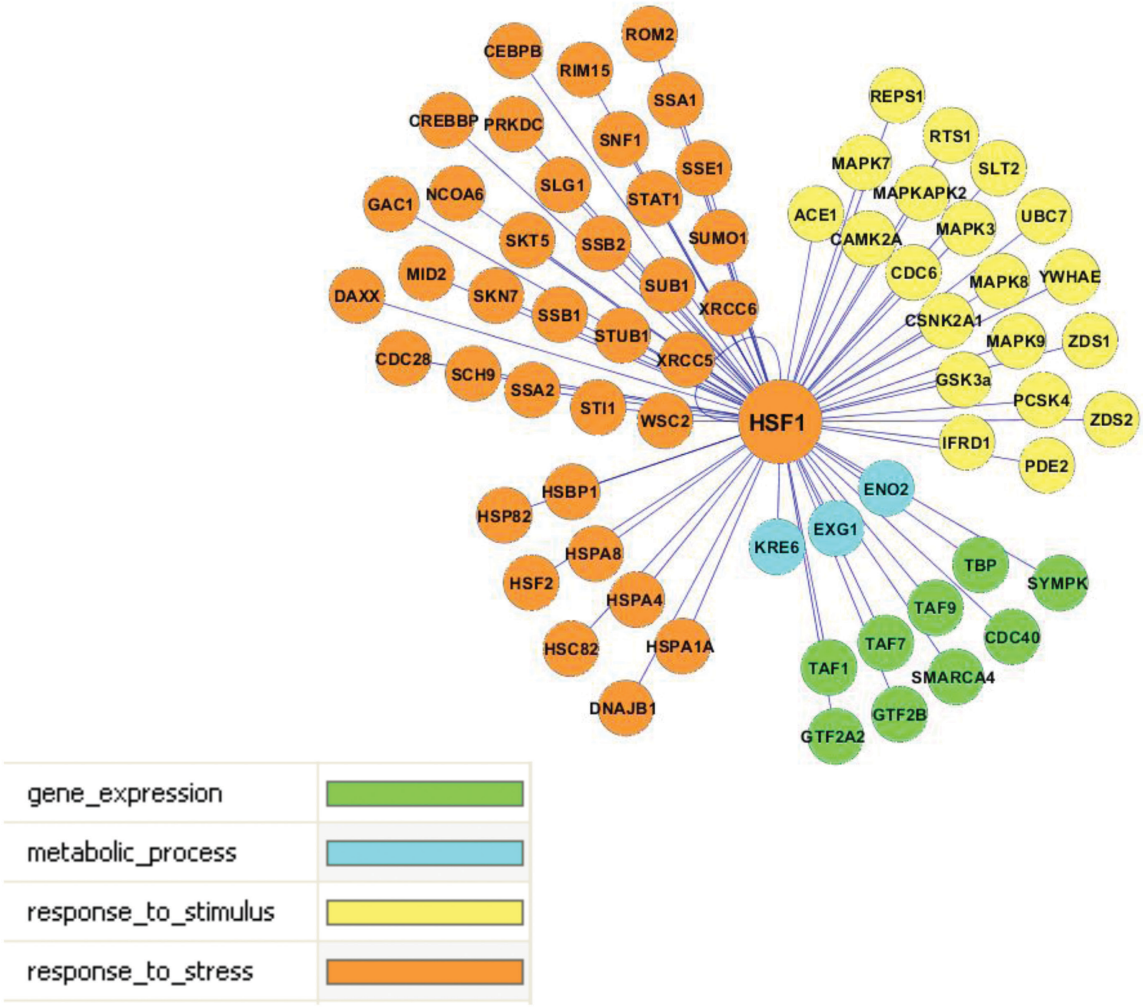

Supplemental Figure 1: Immediate interacting partners of HSF1 as mined from the iHOP interactome database.

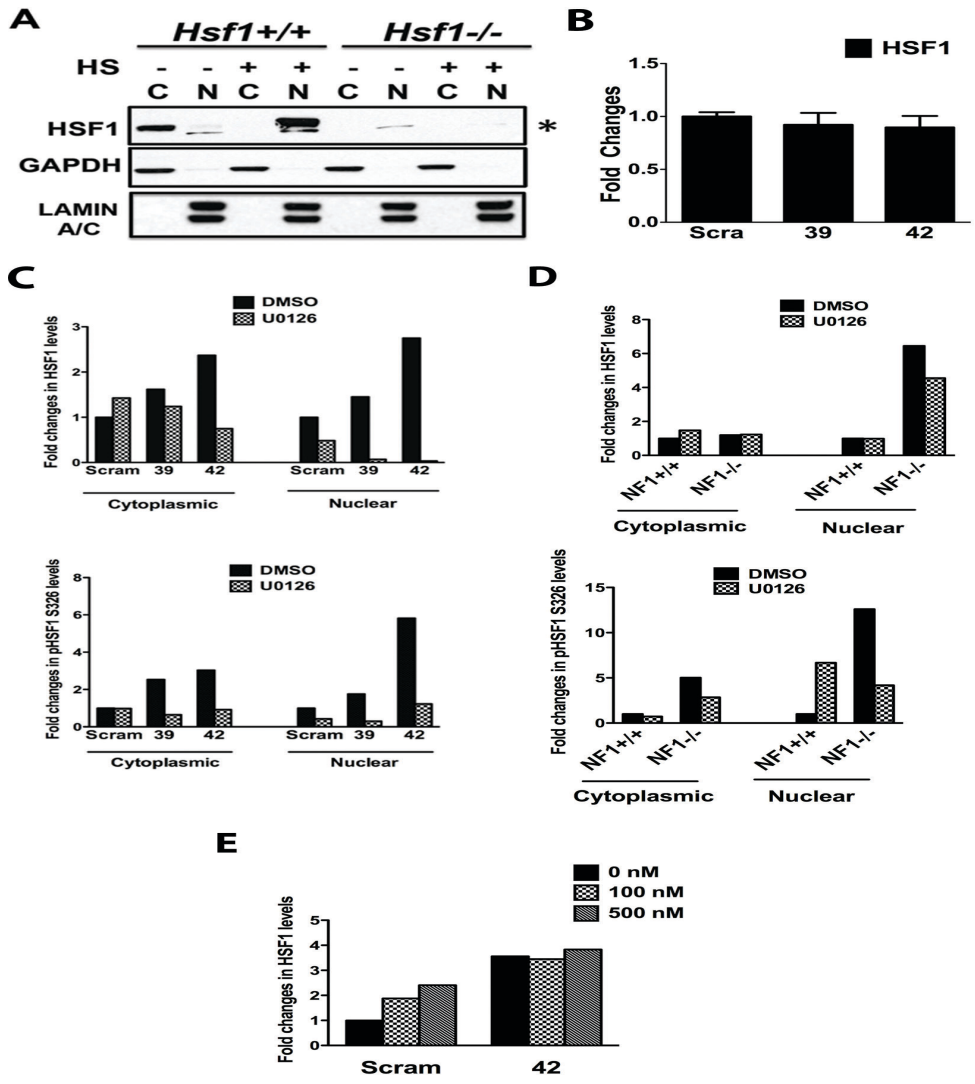

Supplemental Figure 2: (**A**) Immunoblot demonstrating marked HSF1 translocation from the cytoplasm to nucleus following classical heat-shock (43^{0}C for 30 min) of *Hsf1*+/+ wild-type MEF. *Hsf1*-/- MEFs were analyzed in parallel as a specificity control for HSF1 immunoblotting. The cytosolic protein GAPDH and nuclear lamins A/C were blotted as controls for the fractionation procedure. (**B**) HSF1 mRNA levels in *Nf1*-knockdown cells. (**C** and **D**) Densitometric quantitation of immunoblot (Figure 2B and 2D) by ImageJ software showing reduction of HSF1 nuclear localization and pHSF1 Ser326 following U0126 treatment. The densities of cytoplasmic and nuclear HSF1 and pHSF1 Ser326 were normalized against the densities of LDH and Lamin A/C respectively. The normalized protein levels of NF1-deficient cells (#39 and 42 or *Nf1-/-* cells) relative to those of the control cells (Scramble or *Nf1+/+* cells) were expressed as fold changes. (**E**) Densitometric quantitation of HSF1 levels in Figure 2H.

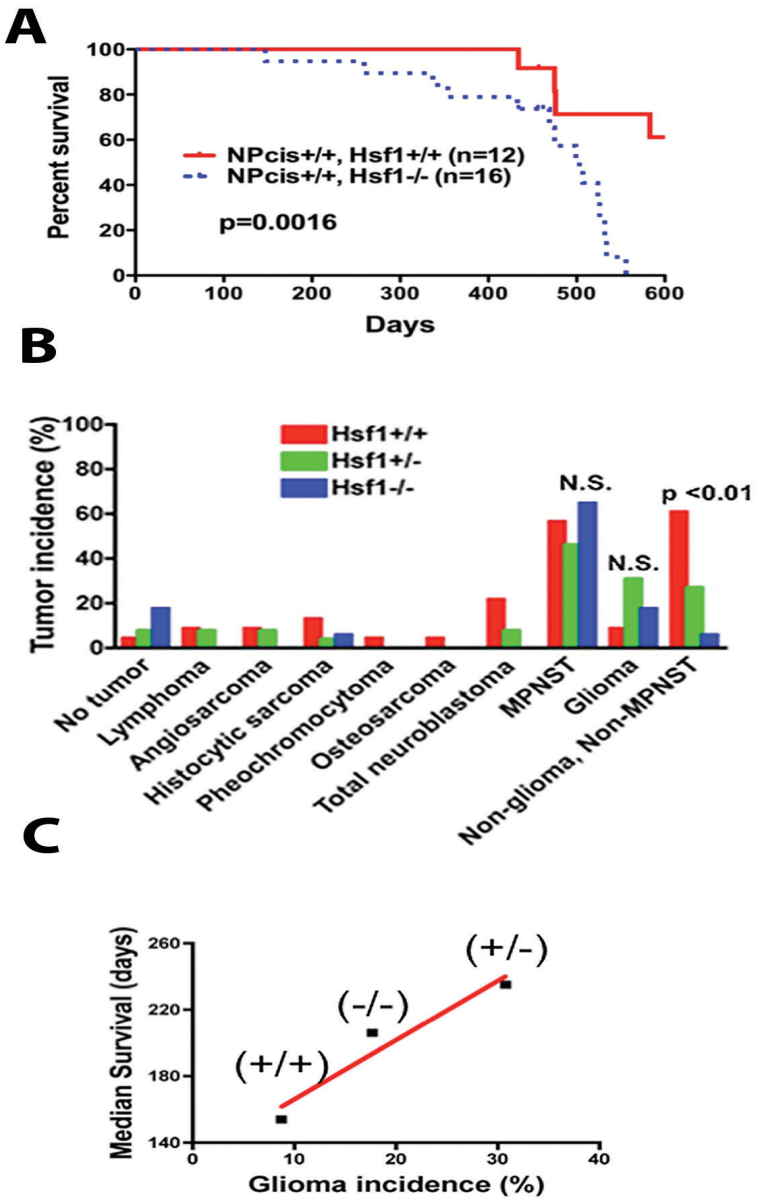

Supplemental Figure 3: (**A**) Kaplan-Meier analysis shows that *Hsf1*-/- mice have shorter overall survival than *Hsf1*+/+ mice in the absence of *Nf1* alterations. (**B**) The incidence of most spontaneously arising tumor types in *NPcis* mice is modified by *Hsf1*. Compared to *Hsf1* wild-type mice, the combined incidence of tumor histologies other than MPNST and glioma is significantly decreased in *Hsf1* null and hemizygous knockout mice (Chi-square test). (**C**) The occurrence of glioma positively correlates with survival, which is prolonged by *Hsf1*-deficiency (r^2=0.9283).

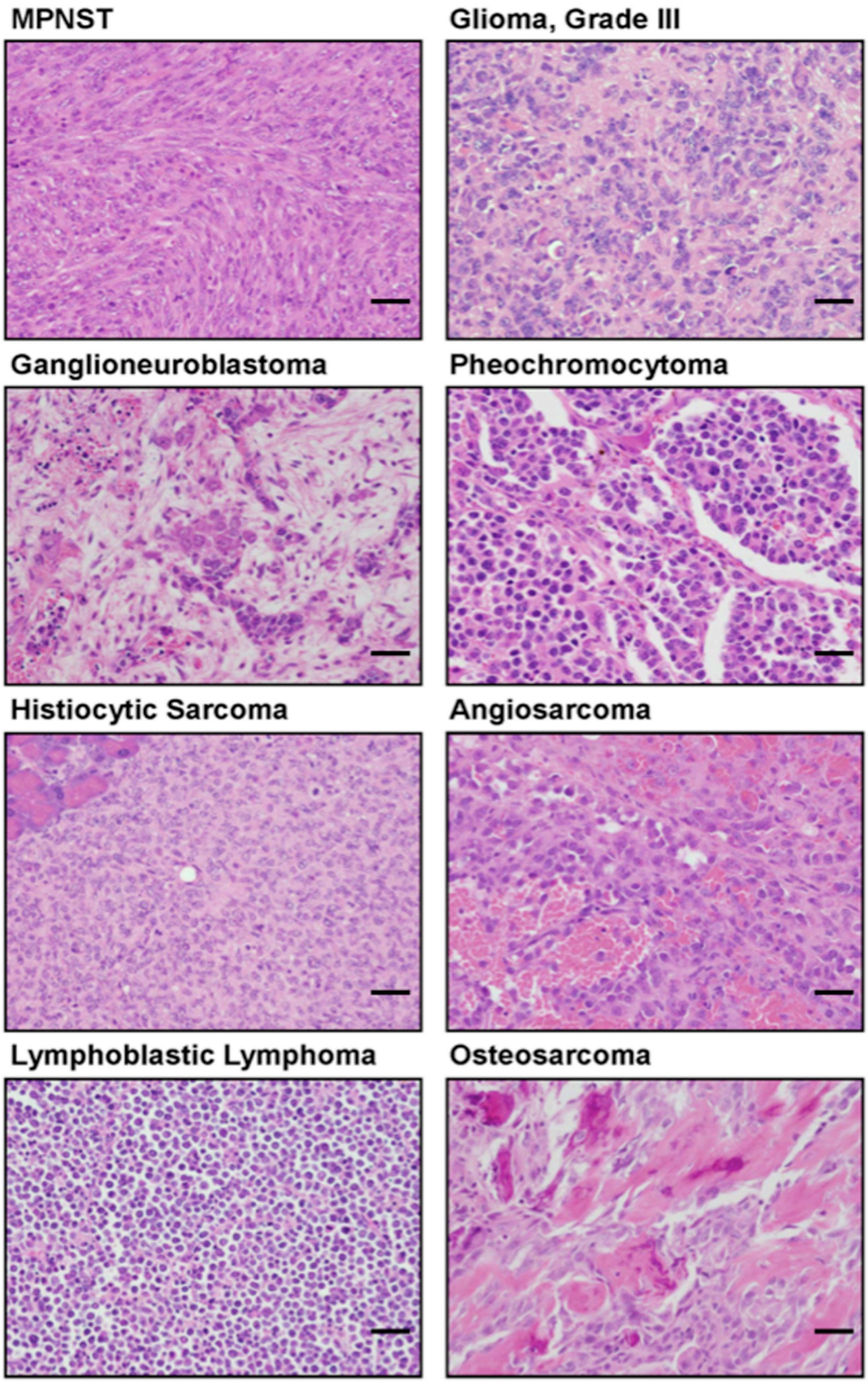

Supplemental Figure 4: *NPcis* mice develop a broad range of malignant tumors. Representative photomicrographs of H&E-stained sections demonstrate characteristic histologies for the indicated tumor types. All images were acquired at the same magnification. Scale bar, 50 μm.

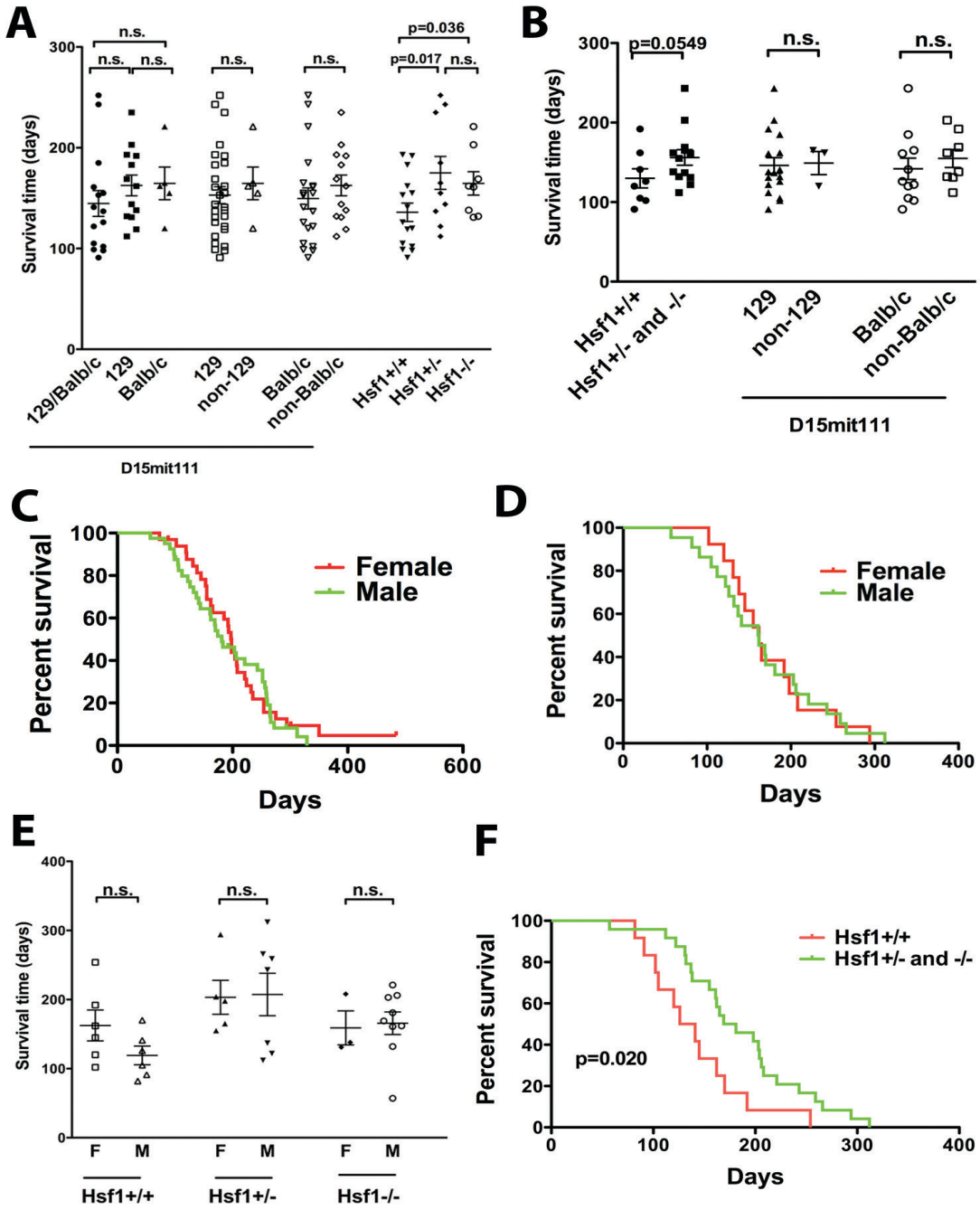

Supplemental Figure 5: (**A**) The previously mapped genetic modifier on chromosome 15, *Nstr2*, did not significantly affect the survival of *NPcis* mice. Total 33 tumors harvested from all 3 *Hsf1* experimental groups were genotyped using the simple-sequence length polymorphism (SSLP) marker D15mit111 to distinguish between the 129/SvJ and Balb/cJ genetic backgrounds. These mice are divided into groups based on D15mit111 genotypes and their survival times are compared (Student's t-test, one-tailed). (**B**) Mice that developed MPNSTs are divided into groups based on D15mit111 genotypes and their survival times are compared (Student's t-test, one-tailed). (**C**) Sex did not significantly affect the survival of all *NPcis* mice. (**D**) Sex did not significantly affect the survival of *NPcis* mice that developed MPNSTs. (**E**) Sex also did not significantly affect the survival time of mice developing MPNSTs within the same *Hsf1* genotypic group (Student's t-test, two-tailed). (**F**) In contrast, *Hsf1*-deficient mice that developed MPNSTs had a longer survival than *Hsf1* wild-type mice that developed MPNSTs (p=0.025, Log-rank test).

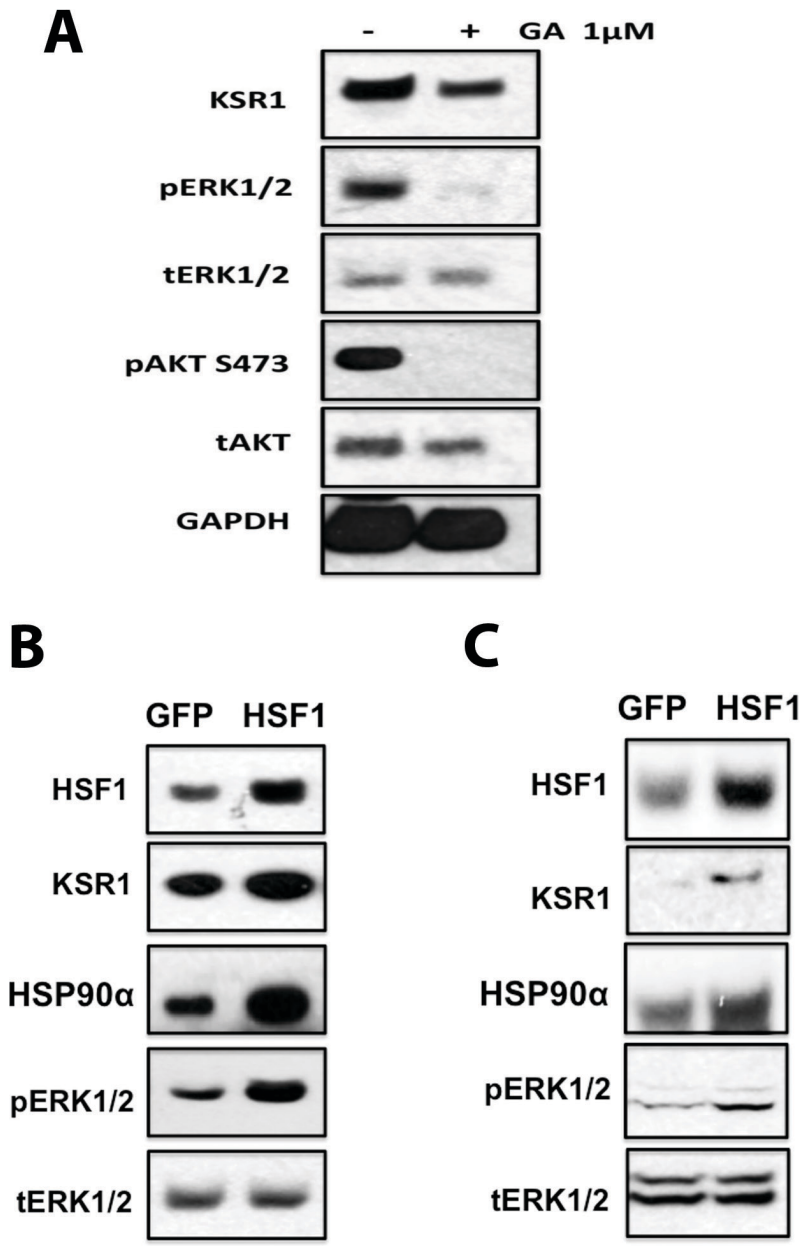

Supplemental Figure 6: **(A)** Decreased levels of KSR1, phospho-ERK1/2, and AKT following HSP90 inhibition. 90-8TL cells were treated overnight with 1μM geldanamycin and harvested for immunoblotting. (**B** and **C**) HSF1 overexpression increases the levels of HSP90α, KSR1 and phospho-ERK1/2 in HEK293 cells (B) and in immortalized MEFs (C). HSF1 overexpression was achieved by either transient transfection in HEK293 cells or stable retroviral infection in MEFs.

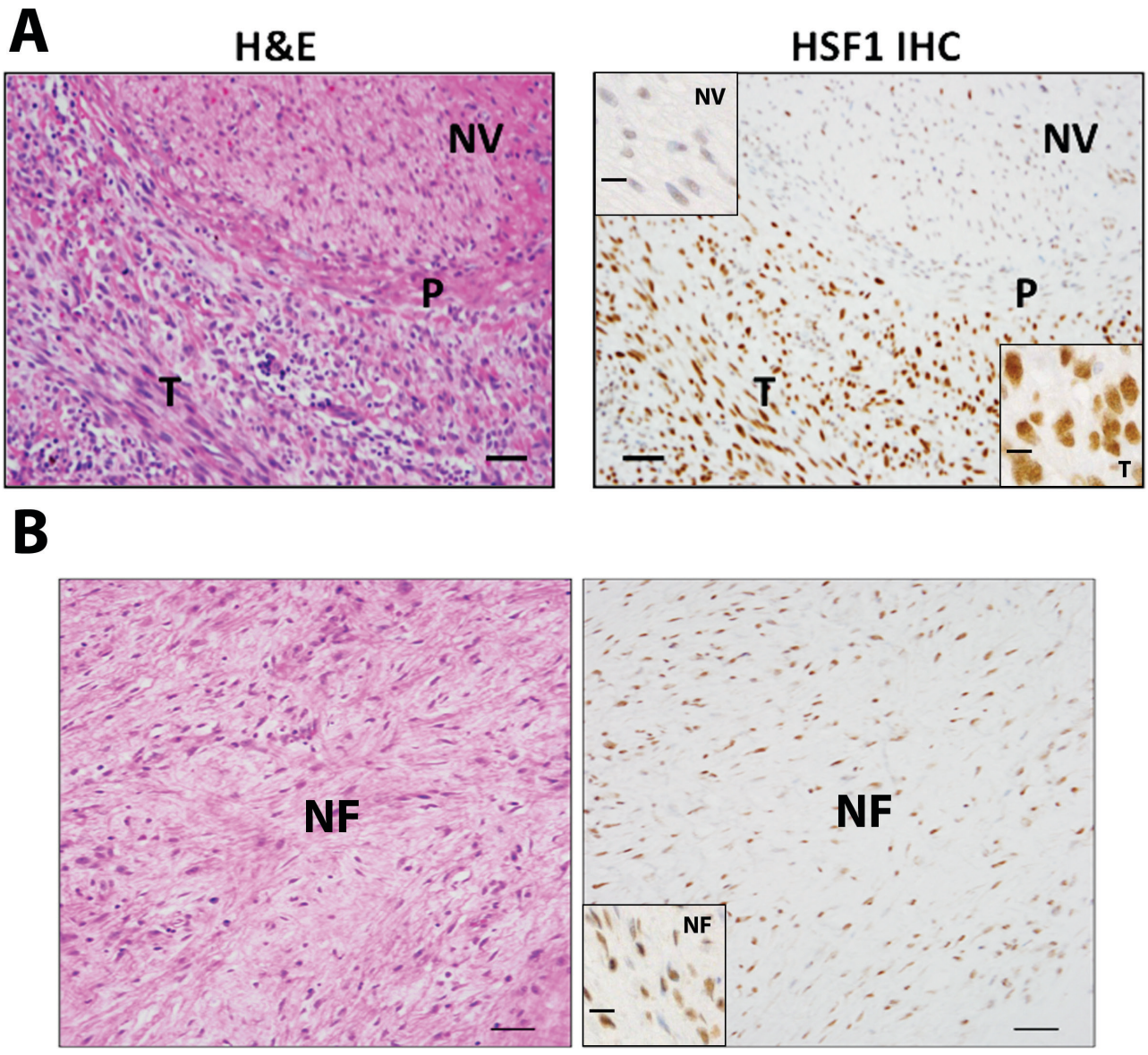

Supplemental Figure 7: HSF1 is highly overexpressed in human MPNST cells from surgical resection specimens. (**A**) H&E stain and HSF1 immunostain of a MPNST tumor section at the same magnification. Scale bar, 50 μm. The cells within the endoneurium of the nerve (NV) and the perineurium (P) show low level expression of HSF1 compared with the malignant cells. Scale bar for the insets, 10 μm. (**B**) H&E stain and HSF1 immunostain of a neurofibroma section at the same magnification. Scale bar, 25 μm. Many cells within benign neurofibroma (NF) show intermediate level expression of HSF1. Scale bar for the inset, 10 μm.

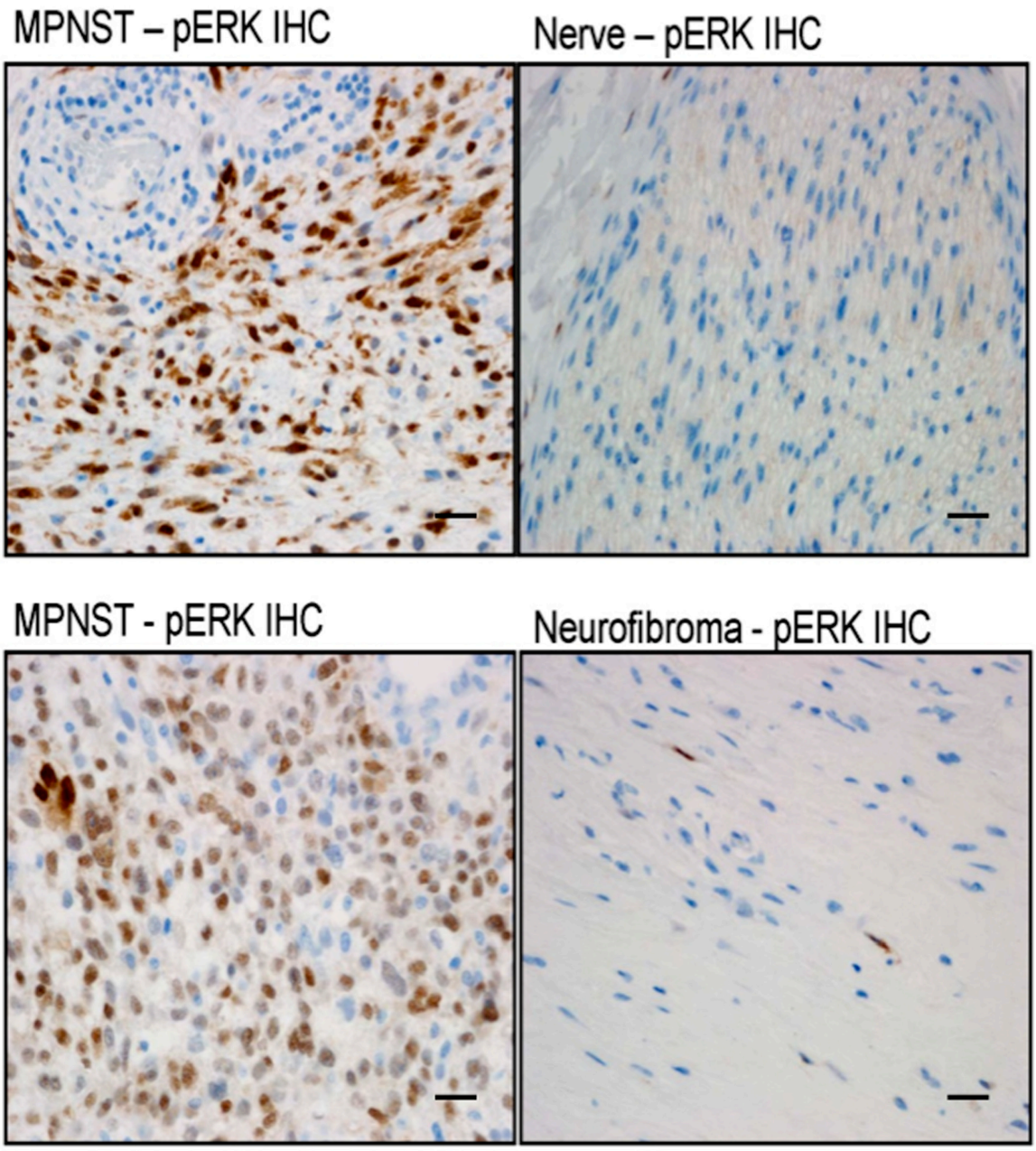

Supplemental Figure 8: Phospho-ERK (pERK) is markedly increased in human MPNSTs compared to normal nerve and benign neurofibroma. Left panels: Representative photomicrographs of tissue sections from two human MPNSTs stained by IHC for pERK (brown signal). Right panels: Sections of nerve and neurofibroma stained under identical conditions show much less pERK immunoreactivity. All sections were counterstained with Mayer hematoxylin (blue) and imaged at identical magnification. Scale bar, 25 μm.

Supplemental Table 1: Summary of all NPcis mice.

ID#	Hsf1	sex	survival days	Tumor types
195	+/+	M	174	Histiocytic sarcoma
197	+/+	F	119	ganglioneuroblastoma
200	+/+	F	197	Autolysis
287	+/+	M	258	Angiosarcoma
288	+/+	M	256	Osteosarcoma,Histiocytic sarcoma,glioma,Angiosarcoma
289	+/+	M	183	ganglioneuroblastoma , Glioma
292	+/+	M	98	Neuroblastoma
297	+/+	F	153	Pheochromocytoma, Rhabdomyosarcoma
300	+/+	M	91	MPNST
302	+/+	M	105	MPNST
307	+/+	F	102	MPNST
308	+/+	F	145	MPNST
311	+/+	F	193	Lymphoblastic lymphoma
330	+/+	M	126	MPNST
373	+/+	M	141	MPNST
378	+/+	M	82	MPNST
382	+/+	F	192	MPNST
388	+/+	M	192	No tumor
408	+/+	F	155	Neuroblastoma
437	+/+	M	170	MPNST
489	+/+	F	120	MPNST, lung adenoma
491	+/+	F	254	MPNST, Lymphoblastic lymphoma
619	+/+	F	162	MPNST
716	+/+	M	99	Composite tumor: Ganglioneuroblastoma/MPNST
124	+/-	F	204	MPNST
126	+/-	M	106	Lymphoma and Angiosarcoma
127	+/-	M	265	Neurofibroma
128	+/-	F	235	Histiocytic Sarcoma, Glioma
130	+/-	F	350	Glioma
131	+/-	F	165	MPNST
132	+/-	M	252	Lymphoblastic Lymphoma
139	+/-	F	185	ganglioneuroblastoma
146	+/-	F	88	No Tumor
148	+/-	M	144	Composite tumor: Ganglioneuroblastoma/MPNST
150	+/-	F	73	Autolysis
151	+/-	F	224	Glioma, lung adenoma
152	+/-	F	155	MPNST
156	+/-	M	272	Autolysis
157	+/-	M	122	MPNST
163	+/-	M	101	No tumor
186	+/-	M	265	GLIOMA
187	+/-	M	243	MPNST, Glioma
189	+/-	M	252	Glioma
198	+/-	F	294	MPNST, Glioma
202	+/-	F	275	Autolysis
203	+/-	M	329	Autolysis
290	+/-	M	112	MPNST
389	+/-	M	137	MPNST
399	+/-	M	266	MPNST
400	+/-	M	312	MPNST
698	+/-	M	260	Glioma
717	+/-	M	259	MPNST
738	+/-	F	198	MPNST
742	+/-	F	198	ANGIOSARCOMA
134	-/-	M	169	MPNST
135	-/-	M	206	MPNST
159	-/-	F	301	No tumor
188	-/-	M	221	MPNST
196	-/-	M	162	MPNST
296	-/-	M	181	MPNST
316	-/-	F	254	Autolysis
371	-/-	F	207	Autolysis
374	-/-	M	161	MPNST
404	-/-	F	221	Histiocytic sarcoma, Glioma
407	-/-	F	131	MPNST
439	-/-	M	57	MPNST
506	-/-	M	293	No tumor
631	-/-	M	203	MPNST
702	-/-	F	138	MPNST
704	-/-	F	208	MPNST, Glioma
706	-/-	M	132	MPNST
710	-/-	F	484	No tumor
711	-/-	F	232	Glioma

Supplemental Table 2: Genotypes of tumors for SSLP markers.

ID#	Hsf1 genotype	D15mit111		D19mit59		Survival days	MPNST
		129/SvJ	Balb/cJ	129/SvJ	Balb/cJ		
197	+/+	+	-	+	-	119	
289	+/+	+	-	+	-	183	
292	+/+	+	+	+	-	98	
297	+/+	+	+	+	-	153	
300	+/+	+	+	+	-	91	Y
302	+/+	+	+	+	-	105	Y
307	+/+	+	+	+	-	102	Y
311	+/+	+	-	+	-	193	
330	+/+	+	+	+	-	126	Y
373	+/+	+	+	+	-	141	Y
382	+/+	+	-	+	-	192	Y
408	+/+	-	+	+	-	155	
489	+/+	-	+	+	-	120	Y
619	+/+	-	+	+	-	162	Y
716	+/+	+	+	+	-	99	
128	+/-	+	-	+	-	235	
131	+/-	-	+	+	-	165	Y
132	+/-	+	+	+	-	252	
139	+/-	+	+	+	-	185	
148	+/-	+	-	+	-	144	
152	+/-	+	+	+	-	185	Y
157	+/-	+	+	+	-	122	Y
187	+/-	+	+	+	-	243	Y
290	+/-	+	-	+	-	112	Y
389	+/-	+	+	+	-	137	Y
134	-/-	+	-	+	-	169	Y
196	-/-	+	-	+	-	162	Y
374	-/-	+	+	+	-	161	Y
404	-/-	-	+	+	-	221	
407	-/-	+	-	+	-	131	Y
631	-/-	+	-	+	-	203	Y
702	-/-	+	-	+	-	138	Y
706	-/-	+	-	+	-	132	Y